https://ntrs.nasa.gov/search.jsp?R=19930082540 2020-06-17T22:00:16+00:00Z

GOVT. DOC.

Y 3.N21/5:6/1865

NACA TN No. 1865

NATIONAL ADVISORY COMMITTEE FOR AERONAUTICS

TECHNICAL NOTE

No. 1865

FURTHER EXPERIMENTS ON THE FLOW AND HEAT TRANSFER IN A HEATED TURBULENT AIR JET

By Stanley Corrsin and Mahinder S. Uberoi

California Institute of Technology

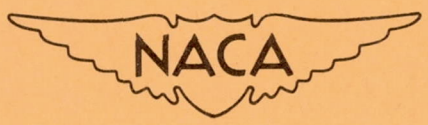

Washington
April 1949

CONN. STATE LIBRARY

APR 28 1949

BUSINESS, SCIENCE & TECHNOLOGY DEP'T.

NATIONAL ADVISORY COMMITTEE FOR AERONAUTICS

TECHNICAL NOTE NO. 1865

FURTHER EXPERIMENTS ON THE FLOW AND HEAT TRANSFER IN A HEATED TURBULENT AIR JET

By Stanley Corrsin and Mahinder S. Uberoi

SUMMARY

Measurements have been made of the mean total-head and temperature fields in a round turbulent jet with various initial temperatures. The results show that the jet spreads more rapidly as its density becomes lower than that of the receiving medium, even when the difference is not sufficiently great to cause measurable deviations from the constant-density, dimensionless, dynamic-pressure profile function. Rough analytical considerations have given the same relative spread.

The effective "turbulent Prandtl number" for a section of the fully developed jet was found to be equal to the true (laminar) Prandtl number within the accuracy of measurement.

Measurements of turbulence level (u', v'), temperature fluctuation level ϑ', and temperature-velocity correlation $\overline{\vartheta u}$ permit a comparison of their relative magnitudes.

Direct measurements have been made of the double correlations $\overline{uv}$ and $\overline{\vartheta v}$ across a section of the fully developed jet, and the shear-stress and heat-transfer distributions have been computed therefrom. Finally, these last-mentioned measurements have permitted a determination of the distribution of turbulent Prandtl number across the jet, and these values agree quite well on the average with the effective value computed from mean velocity and temperature alone.

INTRODUCTION

The present work is concerned with two particular problems on the flow of round, low-velocity, turbulent jets: (a) The effect of mean-density differences upon the rate of spread of the jet, which can be examined through the average velocity and density fields; (b) the relative rates of transfer of heat and momentum in a heated jet, which must involve a study of fluctuations in velocity and temperature as well as average fields.

Problem (a) has been investigated experimentally by Pabst (references 1 and 2), Von Bohl (reference 2), and others. Some British results consist of a few rough measurements made in the course of a different

investigation and, unfortunately, the German reports are available only in practically illegible form, so that a thorough reading has not been feasible. These references arrived when the present investigation was in progress and substantiated the result, discussed in detail in the body of the paper, that reduction in density of jet relative to receiving medium increases the rate of spread.

Theoretical analysis of the two-dimensional, variable-density jet has been attempted by Hu (reference 3), using the momentum-transfer theory. However, he has begun by assuming the constant-density characteristics of linear jet spread and inverse parabolic decrease in axial velocity and therefore has not actually solved the variable-density problem.

Goff and Coogan (reference 4) and Abramovich (reference 5) have solved the two-dimensional, variable-density, single-mixing zone, by momentum-transfer and vorticity-transfer theories, respectively. The former analysis involves the drastic assumption of a discontinuous density field.

In general, however, the shortcomings of the theory of mixing length and the more recent theory of constant exchange coefficient, discussed briefly by Liepmann and Laufer (reference 6), render such analyses useful perhaps only for qualitative results. In fact, as illustrated in reference 6, equally useful results in shear flow problems are obtainable with appreciably less difficulty by the use of the integrated equations of motion, with reasonable guesses for the shape of velocity and/or shear profiles.

A related method has been used by Ribner (reference 7), who has given an approximate solution for the variable-density round jet in a moving medium by a rather empirical generalization of the method used by Squire and Trouncer (reference 8) in constant-density jets. However, this method employs the shear assumption of the momentum-transfer theory, so that the result, though a saving in labor, cannot be expected to give greater accuracy than the complete momentum-transfer analysis.

In the present report, a very brief and approximate analysis is given for the relative jet spread as a function of density ratio, obtainable without a complete solution of the integral problem.

The problem just noted is different from that of a jet of high subsonic velocity, in which the temperature differences arise from frictional heating. However, since the maximum rate of dissipation of turbulent energy (into heat) in a jet takes place on the jet axis (reference 9), the over-all behavior of a fully developed, turbulent, high-speed, subsonic jet may not be very much different from a lower speed heated jet, if the high-speed jet starts out with the same temperature as the receiving medium. There appear to be no data available on turbulent jets with Mach number approaching unity. Abramovich (reference 5) has also applied the vorticity-transfer theory to an approximate

solution of the high-speed (subsonic), plane, single-mixing region with the same stagnation temperature for moving and stationary mediums.

The present investigation on problem (a) has been undertaken primarily to determine experimentally the effect of density difference upon the jet spread. Another matter of interest is the possible deviation from simple geometrical similarity for large density differences.

Somewhat more work has been previously done on the simple phases of problem (b), the relative rates of heat and momentum transfer in a round turbulent jet. The first systematic measurements of velocity and temperature distribution were apparently made by Ruden (reference 10), who found that the temperature distribution is appreciably broader than the velocity distribution in the fully developed region. A more detailed investigation of the kinematic quantities, including turbulence level near the axis, was carried out by Kuethe (reference 11). The results of these two investigations have been verified and extended by one of the present writers (reference 12).

Since there exists no satisfactory theory of turbulent shear flow, naturally there is none for heat transfer in turbulent shear flow. Most of the theoretical work has been done on channel and boundary-layer flows, with the heat transfer set up in direct analogy to the momentum transfer. The empirical factor connecting the two is, of course, exactly the quantity that a satisfactory theory must predict.

For turbulent jets, momentum-transfer considerations lead to identical curves for velocity and temperature distributions (reference 13), whereas the modified vorticity-transfer theory leads to the qualitatively correct result (reference 14) that heat diffuses more rapidly than momentum. Quantitatively, however, this result is considerably in error (reference 12).

Clearly, no satisfactory investigation, either experimental or theoretical, of a turbulent flow phenomenon can be made without consideration of the fluctuations as well as the mean distributions. In the round turbulent jet, fairly detailed measurements have been made of the fluctuation kinematic quantities (reference 12), but no previous investigations appear to have included the significant quantities involving temperature fluctuations. Since a hot-wire technique for the simultaneous measurement of temperature and velocity fluctuations has recently been developed (references 15 and 16), it is now possible to study turbulent heat transfer from the points of view of both mean and fluctuating variables.

At the present time, a weakness of the new measuring technique is the uncertainty of the detailed physical form of King's equation (reference 17) for the heat loss from a fine wire to a flowing fluid. A brief discussion is given in appendix A of reference 16. The results presented in the present report indicate that, at least for variable temperature applications, King's equation may be quantitatively satisfactory.

The first measurements of temperature fluctuation level were made in 1946, in connection with the preliminary phases of the present

investigation. However, deviations from rectangularity in the initial jet temperature distribution prompted the construction of a completely new hot-jet unit, used in all measurements presented herein, and the preliminary measurements have not been published.

Measurements of mean total-head and temperature distributions at various jet temperatures have been made in order to find out if there is any appreciable change in the relative rates of heat and momentum transfer with absolute temperature, over a moderate range.

Finally, it should be noted that investigations of heat transfer in turbulent shear flow are important not only for the immediate results but also as a means of studying the turbulent motion itself.

This investigation was conducted at the California Institute of Technology under the sponsorship and with the financial assistance of the National Advisory Committee for Aeronautics. The authors would like to acknowledge the assistance of Dorothy Kerns, Beverly Cottingham, Sally Rubsamen, and Betsy Barnhart in computing the results and drawing the final figures for this report.

SYMBOLS

d	diameter of orifice (1 inch)
x	axial distance from orifice
r	radial distance from jet axis
$\bar{U}$	axial component of mean velocity
$\bar{V}$	radial component of mean velocity
$\bar{U}_{max}$	maximum $\bar{U}$ at a section on jet axis
$\bar{U}_o$	maximum $\bar{U}$ in the jet (i.e., in the potential cone)
q	dynamic pressure $\left(\frac{1}{2}\bar{\rho}\bar{U}^2\right)$
q_{max}	maximum dynamic pressure at a section
q_o	maximum dynamic pressure in the jet
$\bar{T}_a$	mean absolute temperature at a point in the flow
T_r	absolute temperature of the receiving medium

T_o	absolute initial jet temperature
$\bar{\theta} = \overline{T}_a - T_r$	
$\bar{\theta}_{max}$	maximum $\bar{\theta}$ at a section
$\bar{\theta}_o$	maximum θ in the jet $(T_o - T_r)$
u	axial component of instantaneous velocity fluctuation
v	radial component of instantaneous velocity fluctuation
ϑ	instantaneous temperature fluctuation
$u' = \sqrt{\overline{u^2}}$	
$v' = \sqrt{\overline{v^2}}$	
$\vartheta' = \sqrt{\overline{\vartheta^2}}$	
r_1	at any section, the value of r for which $q = \frac{1}{2} q_{max}$
r_2	at any section, the value of r for which $\overline{U} = \frac{1}{2} \overline{U}_{max}$
r'	at any section, the value of r for which $\bar{\theta} = \frac{1}{2} \bar{\theta}_{max}$
P	total pressure
ρ	air density
$\overline{\rho}$	mean density at a point in the flow (at $\overline{T}_a$)
ρ'	density fluctuation
$\overline{\rho}_{min}$	minimum $\overline{\rho}$ at a section on the axis
ρ_o	minimum ρ in the jet (at T_o)
ρ_∞	density of receiving medium (at T_r)
μ	viscosity coefficient of air
ν	kinematic viscosity (μ/ρ)
k	thermal conductivity of air
c_p	specific heat of air at constant pressure

σ Prandtl number

τ shear stress

Q heat transfer per unit area

ϵ turbulent exchange coefficient

β turbulent heat-transfer coefficient

σ_t "turbulent Prandtl number" $\left(\frac{c_p \epsilon}{\beta}\right)$

$\overline{\sigma}_t$ average or effective σ_t across a section of the jet

Δ "momentum diameter" of jet $\left(\Delta = 2\sqrt{2}\left(\int_0^\infty \frac{q}{q_{max}} r\, dr\right)^{1/2}\right)$

Δ_1 Δ at a section in a constant-density jet

Δ_θ "thermal diameter" of hot jet

$$\left(\Delta_\theta = 2\sqrt{2}\left(\int_0^\infty \frac{\overline{\rho}}{\overline{\rho}_{min}} \frac{\overline{U}}{\overline{U}_{max}} \frac{\overline{\theta}}{\overline{\theta}_{max}} r\, dr\right)^{1/2}\right)$$

$R_{\vartheta u} = \dfrac{\overline{\vartheta u}}{\vartheta' u'}$

$R_{\vartheta v} = \dfrac{\overline{\vartheta v}}{\vartheta' v'}$

$R_{uv} = \dfrac{\overline{uv}}{u' v'}$

} double correlation coefficients at a point

e instantaneous hot-wire voltage fluctuation

α, γ, δ sensitivity of skew wire to ϑ, u, and v fluctuations, respectively

EQUIPMENT

Aerodynamic Equipment

The 1-inch hot-jet unit is shown schematically in figure 1. The three-stage axial blower (reference 18) is driven by a 2-horsepower variable-frequency motor, operated at a fraction of rating. Heat is added through two double banks of coils of No. 16 Nichrome wire. As can be seen in the sketch, a good part of the heated air is ducted around the outside of the jet-air pipe in order to maintain a flat initial temperature distribution in the jet. A blower is used to help the air through this secondary heating annulus. Since this auxiliary air is not ducted back into the main blower intake, heat is discharged from the annulus at an appreciable rate and is exhausted outside of the building to minimize room-temperature rise.

The relatively high velocity section between heaters and final pressure box promotes adequate mixing behind the grid to insure a uniform initial jet-temperature distribution. An earlier, simpler unit, mentioned in the INTRODUCTION, had the heating coils in the final (and only) pressure box; as a result, the Reynolds number of the coil wire and even that of an extra ceramic grid were too low to produce turbulent mixing.

The complete unit is photographed in figure 2(a), and figure 2(b) is a close-up of the asbestos orifice plate and the traversing mechanism.

Runs have been made at orifice velocities between 65 and 115 feet per second and at orifice-temperature differences between 0° C and 385° C. The initial dynamic-pressure distribution (fig. 3) is effectively rectangular, and the initial temperature distribution deviates from that only slightly.

Measuring Equipment

The measuring instruments used were: Hypodermic-needle total-head tube, Chromel-Alumel thermocouple, and hot-wire anemometer.

The hot wires were nominally 0.00025-inch platinum etched from Wollaston wire. The etched platinum was soft soldered to the tips of small steel needle supports. The anemometer heating circuits and amplifier were designed and built by Carl Thiele in 1941. The circuit is so arranged that hot-wire time constants are determined by superimposing equal alternating-current voltages at two frequencies upon the balanced direct-current bridge.

The amplifier gain is constant to within ±2 percent over a frequency range from below 7 cycles to 7000 cycles. No check was possible at less than 7 cycles since that was the lower limit of the available oscillators.

Compensation for hot-wire lag is achieved by a resistance-inductance network between two stages of the amplifier. For a normal range of wire time constants, the combination of hot wire and properly compensated amplifier is satisfactory over the entire flat range of the uncompensated amplifier. The amplifier output was read on an approximately critically damped wall galvanometer, with a vacuum thermocouple.

Mean total head (i.e., dynamic pressure in a free jet) and mean temperature were photographically recorded simultaneously, by means of an automatic traversing arrangement, used with the total-head tube and thermocouple. The total-head pressure line was run into a small copper bellows which tilted a mirror, thereby deflecting a narrow light beam upon a uniformly moving sheet of sensitized paper. The simultaneous recording of temperature on the paper utilized directly the light beam reflected from the mirrors of a sensitive galvanometer. The galvanometer was critically damped for all sensitivity settings. The possible errors arising from changes in "steady-state" conditions during a continuous unidirectional traverse were investigated by means of a few check runs in the opposite direction; these showed no appreciable difference.

The automatic traversing was accomplished by means of a screw-driven carriage running horizontally along a steel track (fig. 2). The screw was rotated through a gear, worm, and belt drive by a reversible alternating-current motor with wide speed range, operating on a continuously adjustable transformer. The sensitized-paper holder was mechanically connected to the moving carriage, so that the abcissas of the recording curves were equal to the true radial distance. Paper shrinkage in development was found to be negligible. Figure 4 is a typical record. The symmetry axes of total head and temperature are offset laterally because of the necessary distance between tube and thermocouple.

PROCEDURES

Mean Dynamic Pressure

Mean dynamic pressure is effectively the total head in a free jet and was recorded photographically, as described in the previous section. The photo record was faired and traced on cross-section paper. In order to reduce scatter, each traverse finally presented in this report has been averaged from three individual faired runs. Faired curves from typical repeated traverses are plotted together in figure 5 to illustrate the degree of disagreement. These particular runs were made with the old hot-jet unit.

No correction has been made for the effect of velocity and density fluctuations upon the readings, but a brief analysis of this correction is given in appendix A.

Mean Temperature

The temperature was also recorded photographically, as described in the previous section. Since the galvanometer deflection varied linearly with temperature, there was no reading error specifically attributable to the temperature fluctuations.

Mean Velocity

With the assumption of a perfect gas, velocity was computed from dynamic pressure and temperature.

Axial Component of Turbulence

In the cold jet, the axial component of turbulence was measured in the conventional manner with a single hot-wire, about 2 millimeters in length, set normal to the x- and r-directions.

In the hot jet, $\frac{u'}{\overline{U}}$ was measured simultaneously with $\frac{\vartheta'}{\overline{\theta}}$ and $\frac{\overline{\vartheta u}}{\overline{\theta}\,\overline{U}}$, by the technique described in references 15 and 16.

Throughout the report, no correction has been made for the error (in reading fluctuation levels) due to the fact that the fluctuations are not always small, as assumed in the theory of turbulence measurement with hot-wires. However, some extremely brief check measurements, reported in reference 12, indicate that the absolute values may be fairly good, even at levels above 50 percent.

It is important to note that the mean velocity to which the hot wire responds is $\overline{U}_R = \sqrt{\overline{U}^2 + \overline{V}^2}$ rather than simply $\overline{U}$. Therefore the local turbulence level measured, and plotted in the figures, is actually $\frac{u'}{\overline{U}_R}$. However, this differs appreciably from $\frac{u'}{\overline{U}}$ only at the outer edge of the jet, where the flow is not completely turbulent anyway. The distributions of $\frac{u'}{\overline{U}_{max}}$, however, are just that quantity at all points, having been computed from $\frac{u'}{\overline{U}_{max}} = \frac{u'}{\overline{U}_R}\frac{\overline{U}_R}{\overline{U}_{max}}$. The mean velocity distributions plotted in the same figures as the fluctuation measurements are all $\frac{\overline{U}_R}{\overline{U}_{max}}$ and therefore, at the outer edge, are appreciably different from the curves obtained from total-head-tube measurements and plotted in other figures.

Temperature Fluctuation Level

Temperature fluctuation level was measured directly by using a single wire as a pure resistance thermometer.

Radial Component of Turbulence

The radial component of turbulence was measured in the hot jet with an X-type meter made up of two wires (about 3 mm long), the voltage fluctuations of which were subtracted before amplification. Because of almost unavoidable unsymmetry, the meter was slightly sensitive to $\frac{u'}{\overline{U}}$; appropriate correction has been made.

$\overline{\vartheta u}$ Correlation

The $\overline{\vartheta u}$ correlation was measured simultaneously with $\frac{u'}{\overline{U}}$ and $\frac{\vartheta'}{\overline{\theta}}$, as described in references 15 and 16.

$\overline{uv}$ and $\overline{\vartheta v}$ Correlations

The $\overline{uv}$ and $\overline{\vartheta v}$ correlations were measured simultaneously, according to the general procedure given in the foregoing references. The extreme slowness of the measurements precluded the use of a simple inversion procedure for unsymmetry correction (i.e., repetition of readings at a point, with the meter rotated through 180°). Instead, the results were computed directly with the directional sensitivity calibrations of the individual wires.

The mean squares of the fluctuation voltages of the two wires are

$$\overline{e_1^2} = \alpha_1^2\overline{\left(\frac{\vartheta}{\overline{\theta}}\right)^2} + \gamma_1^2\overline{\left(\frac{u}{\overline{U}}\right)^2} + \delta_1^2\overline{\left(\frac{v}{\overline{U}}\right)^2} + 2\alpha_1\gamma_1\frac{\overline{\vartheta u}}{\overline{\theta}\,\overline{U}} + 2\alpha_1\delta_1\frac{\overline{\vartheta v}}{\overline{\theta}\,\overline{U}} + 2\gamma_1\delta_1\frac{\overline{uv}}{\overline{U}^2}$$

$$\overline{e_2^2} = \alpha_2^2\overline{\left(\frac{\vartheta}{\overline{\theta}}\right)^2} + \gamma_2^2\overline{\left(\frac{u}{\overline{U}}\right)^2} + \delta_2^2\overline{\left(\frac{v}{\overline{U}}\right)^2} + 2\alpha_2\gamma_2\frac{\overline{\vartheta u}}{\overline{\theta}\,\overline{U}} - 2\alpha_2\delta_2\frac{\overline{\vartheta v}}{\overline{\theta}\,\overline{U}} - 2\gamma_2\delta_2\frac{\overline{uv}}{\overline{U}^2}$$

Since there are two unknowns, readings must be taken at two different hot-wire sensitivities. Then the two pairs of differences give

$$\overline{e_1^2} - \overline{e_2^2} = \left(\alpha_1^2 - \alpha_2^2\right)\overline{\left(\frac{\vartheta}{\bar{\theta}}\right)^2} + \left(\gamma_1^2 - \gamma_2^2\right)\overline{\left(\frac{u}{\bar{U}}\right)^2} + \left(\delta_1^2 - \delta_2^2\right)\overline{\left(\frac{v}{\bar{U}}\right)^2}$$

$$+ 2\left(\alpha_1\gamma_1 - \alpha_2\gamma_2\right)\frac{\overline{\vartheta u}}{\bar{\theta}\bar{U}} + 2\left(\alpha_1\delta_1 + \alpha_2\delta_2\right)\frac{\overline{\vartheta v}}{\bar{\theta}\bar{U}} + 2\left(\gamma_1\delta_1 + \gamma_2\delta_2\right)\frac{\overline{uv}}{\bar{U}^2}$$

$$\overline{e_1'^2} - \overline{e_2'^2} = \left(\alpha_1'^2 - \alpha_2'^2\right)\overline{\left(\frac{\vartheta}{\bar{\theta}}\right)^2} + \left(\gamma_1'^2 - \gamma_2'^2\right)\overline{\left(\frac{u}{\bar{U}}\right)^2} + \left(\delta_1'^2 - \delta_2'^2\right)\overline{\left(\frac{v}{\bar{U}}\right)^2}$$

$$+ 2\left(\alpha_1'\gamma_1' - \alpha_2'\gamma_2'\right)\frac{\overline{\vartheta u}}{\bar{\theta}\bar{U}} + 2\left(\alpha_1'\delta_1' + \alpha_2'\delta_2'\right)\frac{\overline{\vartheta v}}{\bar{\theta}\bar{U}}$$

$$+ 2\left(\gamma_1'\delta_1' + \gamma_2'\delta_2'\right)\frac{\overline{uv}}{\bar{U}^2}$$

Thus, the u, v, and ϑ sensitivities of each wire must be determined separately. From previous measurements, $\overline{\left(\frac{\vartheta}{\bar{\theta}}\right)^2}$, $\overline{\left(\frac{u}{\bar{U}}\right)^2}$, $\frac{\overline{\vartheta u}}{\bar{\theta}\bar{U}}$, and $\overline{\left(\frac{v}{\bar{U}}\right)^2}$ are known, and the foregoing pair of linear equations can be solved simultaneously for the two unknowns $\frac{\overline{\vartheta v}}{\bar{\theta}\bar{U}}$ and $\frac{\overline{uv}}{\bar{U}^2}$.

EXPERIMENTAL RESULTS

The axial distributions of dynamic pressure, temperature, and velocity are given in figures 6 and 7, for the constant-density jet for an initial density ratio $\frac{\rho_\infty}{\rho_0} \approx 2$. Since all three variables decrease more rapidly when jet density is appreciably less than that

of the receiving medium, it is to be expected that the lower-density (hot) jet spreads at a wider angle. This is verified in figure 8, which shows the half total-head diameter $2r_1$ and the half temperature diameter $2r'$ as functions of $\frac{x}{d}$, for these two cases.

In figures 6 and 7 it can be seen that both dynamic and thermal potential cones are shorter for the low-density jet. Since the annular mixing region outside of the potential cone is somewhat similar to a single two-dimensional mixing zone, the nature of the flow in this latter case, with flowing medium less dense than stationary medium, can be inferred.

Figures 9 and 10 show the dimensionless profiles of total head temperature, and velocity at a section 15 diameters from the orifice, for $\frac{\rho_\infty}{\rho_o} \approx 1$ and 2. It is immediately evident that the shape of these functions is not appreciably changed at $\frac{x}{d} = 15$ by a doubling of the initial density ratio. The local maximum density ratios at the section are $\frac{\rho_\infty}{\rho_{min}} \approx 1$ and 1.3, respectively. A verification of the negligible change in total-head profile is given in figure 11, in which all the functions have been fitted at the point $r = r_1$.

For a constant-density jet, it is well known that effective similarity of total-head (or velocity) profiles exists for all values of $\frac{x}{d}$ greater than 7 or 8 (references 11 and 12). This is verified in figure 12. Figure 13 shows that an initial density ratio of 2 is not sufficient to change this result appreciably. The deviation of the total-head distributions for $\frac{x}{d} = 20$ at large values of $\frac{r}{r_1}$ is almost certainly due to inaccuracy of the traced data at a section where even the maximum dynamic pressure gives only about a 1-inch deflection on the photo record.

The fact that the density-ratio range covered in the present series of experiments is insufficient to lead to measurable deviation from simple geometrical similarity is clearly shown by the constancy of $\frac{r'}{r_1}$ and $\frac{\Delta}{r_1}$ in figure 14. However, again it should be pointed out that, although the initial density-ratio range is from 1 to 2, the range of maximum density ratio at this particular section is only from 1 to 1.3.

Although r_1 has been used as a characteristic jet width in most of the previous figures, it is clear that a width definition of greater

physical significance can be made on the basis of momentum flow. The "momentum diameter" of the jet at any section

$$\Delta = 2\sqrt{2}\left(\int_0^\infty \frac{q}{q_{max}} r\, dr\right)^{1/2}$$

is defined as the diameter of a jet of rectangular density and velocity profiles ($\rho = \rho_{min}$ and $\overline{U} = \overline{U}_{max}$), whose total rate of flow of axial momentum is the same as in the actual jet at that section. Since the momentum flow in a free jet is effectively constant, this characteristic diameter is particularly convenient. It is analogous to the momentum thickness of a boundary layer, except that the latter is based on momentum defect.

The ratio of hot-jet momentum diameter at $\frac{x}{d} = 15$ to that of the constant-density jet at the same section (fig. 15) shows a definite increase in jet width as the jet fluid becomes less dense than the receiving medium. A few points obtained with the preliminary hot-jet equipment have been included because this simple unit was able to produce an appreciably higher initial temperature. The result of a rough theoretical analysis of the effect, presented in the next section, is drawn in the same figure.

A comparison between the cold-jet axial u' distribution (fig. 16) and that for an initial temperature difference of 170° C (fig. 17) shows that the sharp rise in turbulence level comes a bit earlier for the low-density jet. Of course, this may be due to an inaccuracy in King's equation and thus may not be a real effect; however, the difference is certainly in the direction that would be anticipated as a result of the more rapid spread and development of the mean motion pattern in the lower density case.

The temperature fluctuation level as measured is everywhere lower than the velocity fluctuation level.

Two qualitative aspects of the fluctuations were observed during these particular measurements: First, extremely regular velocity fluctuations were observed in the potential cone, just as illustrated in reference 13; second, the temperature fluctuations on the jet axis, roughly between $\frac{x}{d} = 3$ and 5, were almost entirely one-sided, although the u fluctuations in that region apparently showed no such tendency. The reason for this behavior is not clear at the time of writing.

In the process of measuring $\frac{u'}{\overline{U}}$ in a flow with simultaneous velocity and temperature fluctuations, the $\overline{\vartheta u}$ correlation results more or less as a byproduct; $\frac{\overline{\vartheta u}}{\overline{\theta}_o \overline{U}_o}$ and the coefficient $R_{\vartheta u} = \frac{\overline{\vartheta u}}{\vartheta' u'}$ are plotted in figure 18. In spite of tremendous experimental scatter, which has even produced occasional negative values for $\overline{\vartheta u}$, it appears that $\overline{\vartheta u} > 0$ in turbulent shear flow. The sign can be obtained by the reasoning (in rough analogy to the kinetic theory of gases) that $\overline{uv}$ has a sign opposite to that of $\frac{\partial U}{\partial r}$ in a normal turbulent shear flow.

Since $\overline{\vartheta u}$ is proportional to the turbulent heat transfer in the main flow direction, it is clearly not of as great interest as the $\overline{\vartheta v}$ correlation. It is, however, of use in the computation of the total-head-tube correction for the effect of velocity and temperature fluctuations (appendix A). No attempt has been made to draw a curve through the experimental points.

A check measurement of the lateral u' distribution in the fully developed constant-density jet, in figure 19, shows reasonable agreement with earlier results (reference 12).

Figure 20 contains lateral traverses of both u' and ϑ' in the hot jet at $\frac{x}{d} = 20$. Again, $\frac{\vartheta'}{\overline{\theta}}$ is everywhere slightly less than $\frac{u'}{\overline{U}}$, but it should be noted that $\frac{\vartheta'}{\overline{\theta}_{max}} > \frac{u'}{\overline{U}_{max}}$ in the outer part of the jet. Perhaps associated with this relative behavior is the fact that, although $\frac{\vartheta'}{\overline{\theta}_{max}}$ has a definite local minimum on the jet axis, $\frac{u'}{\overline{U}_{max}}$ is flat in that region, within the accuracy of measurement.

The coefficient $R_{\vartheta u}$ is apparently more or less constant over the central part of the jet (fig. 21).

Considerably more complete measurements have been made at $\frac{x}{d} = 15$ in the hot jet. In addition to u', ϑ', and $\overline{\vartheta u}$ distributions (figs. 22, 23, and 24), there is also a traverse of the lateral component of turbulence $\frac{v'}{\overline{U}}$ and $\frac{v'}{\overline{U}_{max}}$. It may be noticed that, in agreement with figure 24 of reference 12, $v' > u'$ in the immediate vicinity of the axis, and $u' > v'$ *elsewhere*.

The $\overline{uv}$ and $\overline{\vartheta v}$ correlations and correlation coefficients

$$R_{uv} = \frac{\overline{uv}}{u'v'} \quad \text{and} \quad R_{\vartheta v} = \frac{\overline{\vartheta v}}{\vartheta' v'}$$

are plotted in figure 25. There is a great deal of experimental scatter but the general behaviors are clear. Furthermore, it is obvious that $R_{\vartheta v} > R_{uv}$, which is exactly what is to be anticipated from the fact that the rate of turbulent heat transfer is known (from the mean velocity and temperature curves) to be greater than the momentum transfer.

Of course, because of the effect of density fluctuations, the turbulent shear and heat transfer cannot be expressed simply as $-\bar{\rho}\overline{uv}$ and $-c_p\bar{\rho}\overline{\vartheta v}$, respectively. A brief calculation (appendix D, reference 16) leads to the approximate expressions

$$\tau = -\bar{\rho}\overline{uv} + \bar{\rho}\frac{\overline{U}}{\overline{T}_a}\overline{\vartheta v}$$

$$Q = c_p\bar{\rho}\left(1 - \frac{\overline{\theta}}{\overline{T}_a}\right)\overline{\vartheta v}$$

In figure 26, the shear stress and heat transfer are plotted in the dimensionless forms

$$\frac{\tau}{\overline{\rho}_{min}\overline{U}_{max}^2} = -\frac{T_r + \overline{\theta}_{max}}{\overline{T}_a}\left(\frac{\overline{uv}}{\overline{U}_{max}^2}\right) + \frac{\overline{\theta}_{max}\left(T_r + \overline{\theta}_{max}\right)}{\overline{T}_a^2}\frac{\overline{U}}{\overline{U}_m}\left(\frac{\overline{\vartheta v}}{\overline{\theta}_{max}\overline{U}_{max}}\right)$$

$$\frac{Q}{c_p\overline{\rho}_{min}\overline{\theta}_{max}\overline{U}_{max}} = -\frac{T_r + \overline{\theta}_{max}}{\overline{T}_a}\left(1 - \frac{\overline{\theta}}{\overline{T}_a}\right)\left(\frac{\overline{\vartheta v}}{\overline{\theta}_{max}\overline{U}_{max}}\right)$$

ANALYTICAL CONSIDERATIONS

Jet Width as a Function of Initial Density Ratio

As mentioned in the INTRODUCTION, integrated equations, along with dimensional reasoning in transforming the variables, can usually be made to yield solutions describing the integral behavior of a shear flow.

The two-dimensional integrated momentum and mechanical-energy equations have been derived by Liepmann and Laufer (reference 6). An identical procedure leads to the axially symmetrical forms, omitting bars for mean motion.

Momentum:

$$\frac{d}{dx}\int_a^b \rho U^2 r\,dr - \rho_b U_b{}^2{}_b \frac{db}{dx} + \rho_a U_a{}^2{}_a \frac{da}{dx} + \left[\rho r U V\right]_a^b = \left[r\tau\right]_a^b \qquad (1)$$

mechanical energy:

$$\frac{1}{2}\frac{d}{dx}\int_a^b \rho U^3 r\,dr - \frac{1}{2}\rho_b U_b{}^3 \frac{db}{dx} + \frac{1}{2}\rho_a U_a{}^3{}_a \frac{da}{dx} + \frac{1}{2}\left[\rho r U^2 V\right]_a^b$$

$$= \left[rU\tau\right]_a^b - \int_a^b r\tau \frac{\partial U}{\partial r}\,dr \qquad (2)$$

A similar treatment of the heat-transfer equation, with specific heat assumed independent of temperature, gives, again omitting the bars since all quantities are mean quantities,

$$\frac{d}{dx}\int_a^b \rho U\theta r\,dr - \rho_b U_b \theta_b{}_b \frac{db}{dx} + \rho U_a \theta_a{}_a \frac{da}{dx} + \left[\rho r\theta V\right]_a^b = \frac{1}{c_p}\left[rQ\right]_a^b \qquad (3)$$

For the particular case of a free jet entering an infinite medium at rest, these three equations simplify to

$$\int_0^\infty \rho U^2 r \, dr = \text{Constant} = \frac{M}{2\pi} \tag{4}$$

$$\frac{d}{dx} \int_0^\infty \rho U^3 r \, dr = -2 \int_0^\infty r\tau \frac{\partial U}{\partial r} \, dr \tag{5}$$

$$\int_0^\infty \rho U \theta r \, dr = \text{Constant} = \frac{N}{2\pi} \tag{6}$$

where the integrals have been extended to infinity to permit the use of asymptotic velocity- and temperature-profile assumptions. If finite width functions are used, the integrals can be extended only to some judiciously chosen b. It should also be mentioned that in the integral continuity equation, which can be used to find the radial velocity V_b, the finite limit is essential.

Equation (4) expresses the condition of constant total flux of momentum across all planes perpendicular to the jet axis in the absence of a pressure gradient. Equation (5) equates the rate of decrease of mean-flow kinetic energy per unit time to the rate of production of heat (in the laminar case) or of turbulent kinetic energy (in the turbulent case).

Equation (6), expressing the constancy of heat flow across all planes perpendicular to the x-axis, is of course the thermal part of the energy equation, for the case in which heat production by viscous action is negligible. When the density variation is isothermal and due to the use of a jet fluid different from the receiving medium, equation (6) is replaced by what may be considered the conservation of mass-flow defect or excess:

$$\int_0^\infty (\rho - \rho_\infty) U r \, dr = \text{Constant} = \frac{M'}{2\pi} \tag{7}$$

and, in fact, equation (7) is easily obtainable from equation (6) with the equation of state of a perfect gas, assuming constant pressure.

If there is introduced an appropriate dimensionless variable, along with reasonable assumptions for the dimensionless velocity and density profiles, equations (4), (5), and (7) can be solved for $U_{max}(x)$, $\rho_{min}(x)$, and the momentum diameter $\Delta(x)$. The integrated continuity equation can be used to solve for radial velocities. Although τ can in principle be determined from the two assumed functions (see, for example, references 6 and 12) it is sometimes more convenient to make a reasonable assumption for this distribution also.

The purpose of the present analysis is only to obtain an approximate expression for $\frac{\Delta}{d}$ as a function of $\frac{\rho_\infty}{\rho_o}$, for a fixed value of $\frac{x}{d}$; it turns out that this can be done without the mechanical-energy equation.

The velocity and density profiles are represented by dimensionless functions

$$\frac{U}{U_{max}} = f(\eta) \quad \text{and} \quad \frac{\rho - \rho_\infty}{\rho_{min} - \rho_\infty} = g(\eta) \tag{8}$$

where η is the appropriate similarity parameter. It can be shown, by resulting inconsistencies in the two equations to be solved, that simple geometrical similarity does not exist. In fact, it seems physically evident that the profile functions should vary with the local density ratio. Taking

$$\eta = \frac{2r}{\Delta} F\left(\frac{\rho_{min}}{\rho_\infty}\right)$$

the form of F is obtained by substituting equation (8) and the definition of momentum diameter

$$\frac{\pi\Delta^2}{4} \rho_{min} U_{max}^2 = M$$

into equation (4). Then,

$$2\pi \int_0^\infty \left[\rho_\infty + (\rho_{min} - \rho_\infty)g\right] U_{max}^2 f^2 \frac{\Delta}{4F^2} \eta \, d\eta = \frac{\pi\Delta^2}{4} \rho_{min} U_{max}^2$$

which gives

$$F = \sqrt{2}\left[I_2 + (I_1 - I_2)\frac{\rho_\infty}{\rho_{min}}\right]^{1/2}$$

where I_1 and I_2 are pure numbers dependent upon the assumed velocity and density functions

$$I_1 = \int_0^\infty \eta f^2(\eta)\, d\eta \quad \text{and} \quad I_2 = \int_0^\infty \eta f^2(\eta) g(\eta)\, d\eta$$

Thus, the proper similarity parameter is

$$\eta = 2\sqrt{2}\,\frac{r}{\Delta}\left[I_2 + (I_1 - I_2)\frac{\rho_\infty}{\rho_{min}}\right]^{1/2} \tag{9}$$

which is a function of x. If the problem were solved for $\rho_{min}(x)$ and $\Delta(x)$, η could then be expressed in its most suitable form, as a function of r, x, and the initial density ratio.

It is of some interest to inspect the parameter η. For constant-density flow, $\eta = \sqrt{2I_1}\,\frac{2r}{\Delta}$, and simple geometrical similarity exists. For heated turbulent jets it is found that $I_1 > I_2$, since $g(\eta) \leq 1.0$ everywhere. Thus, with ρ_{min} appreciably less than ρ_∞, a particular value of η is reached at smaller r (for fixed Δ) than in the constant-density case.

Substitution of equation (9) into equation (4) merely gives the definition of Δ, which is now written with the explicit expression for M:

$$\rho_{min} U_{max}{}^2 \Delta^2 = \rho_o U_o{}^2 d^2 \tag{10}$$

With equation (9) and the explicit expression for M, equation (7) becomes

$$I_3\,\frac{\rho_{min} U_{max} \Delta^2 (\rho_{min} - \rho_\infty)}{I_1 \rho_\infty + I_2(\rho_{min} - \rho_\infty)} = (\rho_o - \rho_\infty) U_o\, d^2 \tag{11}$$

where

$$I_3 = \int_0^\infty \eta f(\eta) g(\eta)\, d\eta$$

Equations (10) and (11) are to be solved for $\frac{\Delta}{d}$ as a function of $\frac{\rho_o}{\rho_\infty}$, at a particular value of $\frac{x}{d}$. Since there are fewer equations than unknowns, some assumption must be made concerning the axial distribution of either velocity or density. It is convenient to make the simplifying assumption that the dimensionless axial density distribution $\left(\frac{\rho_{min} - \rho_\infty}{\rho_o - \rho_\infty}\right)$ is independent of the initial density ratio.

Then $\frac{U_{max}}{U_o}$ from equation (10) is substituted into equation (11), and all ρ_{min}'s are expressed in terms of $\left(\frac{\rho_{min} - \rho_\infty}{\rho_o - \rho_\infty}\right)$. After further approximation by the use of the first two terms of binomial expansions, the following result is obtained:

$$\frac{\Delta}{d} = \frac{I_1}{I_3}\sqrt{\frac{\rho_\infty}{\rho_o}}\left[1 + \left(\frac{I_2}{I_1} - \frac{1}{2}\right)\left(\frac{\rho_{min} - \rho_\infty}{\rho_o - \rho_\infty}\right)\left(\frac{\rho_o}{\rho_\infty} - 1\right)\right] \tag{12}$$

or

$$\frac{\Delta}{\Delta_1} = \sqrt{\frac{\rho_\infty}{\rho_o}}\left[1 + \left(\frac{I_2}{I_1} - \frac{1}{2}\right)\left(\frac{\rho_{min} - \rho_\infty}{\rho_o - \rho_\infty}\right)\left(\frac{\rho_o}{\rho_\infty} - 1\right)\right] \tag{12a}$$

where Δ_1 is the momentum width at the same axial distance for the constant-density jet, and where the desired $\frac{x}{d}$ is obtained by choosing $\left(\frac{\rho_{min} - \rho_\infty}{\rho_o - \rho_\infty}\right)$ according to temperature measurements in the constant-density case. Thus it is clear that, as may be intuitively anticipated, the jet spreads at a wider angle when the jet fluid is less dense than the receiving medium, and vice versa.

A numerical value for $\frac{I_2}{I_1}$ is obtained by computation from velocity and temperature distributions in the measurements of the constant-density case. These give $\frac{I_2}{I_1} = 0.727$ and equation (12a) is plotted in figure 15 for comparison with the experimental results. Because of the rather severe approximation, agreement is not good. The complete solution of equations (4), (5), and (7), however, is rather laborious.

Measure of Turbulent Prandtl Number

One of the more important and interesting problems in the study of turbulent shear flow is the relation between momentum transfer and heat transfer.

For laminar flows, the ratio of momentum to heat transfer is directly computable from the kinetic theory of gases and is conventionally described by the well-known Prandtl number

$$\sigma = \frac{c_p \mu}{k}$$

For nearly perfect gases, σ is only slowly variable with temperature over a wide range since c_p is nearly constant and μ and k vary nearly proportionally. For effectively isothermal laminar flow, c_p, μ, and k are individually constant over the entire flow field.

The quantity analogous to σ, for turbulent flow, is

$$\sigma_t = \frac{c_p \epsilon}{\beta} \tag{13}$$

which may be termed the "turbulent Prandtl number." The "eddy viscosity" and "eddy conductivity," as defined by Dryden (reference 19) are

$$\left.\begin{aligned} -\rho\overline{u'v'} &= \epsilon \frac{\partial U}{\partial r} \\ -c_p \rho \overline{\vartheta' v'} &= \beta \frac{\partial \theta}{\partial r} \end{aligned}\right\}^{1} \tag{14}$$

[1] In this section all U's and θ's are mean values.

and if the density fluctuations are negligible, as is the case within the accuracy of the present experiments,

$$\tau = \epsilon \frac{\partial U}{\partial r}$$

$$Q = \beta \frac{\partial \theta}{\partial r}$$

Since ϵ and β are themselves rather artificial quantities, introduced merely in overstrained analogy to laminar flow, it is not to be expected that σ_t has any fundamental physical basis, other than the exact definition given in equation (15). However, in the absence of a satisfactory analysis of turbulent shear flow, it serves as an empirical measure of the ratio of momentum transfer to heat transfer. Although ϵ and β vary from point to point, even in an isothermal turbulent shear flow, the variations in their ratio $(\sim \sigma_t)$ may be of distinct interest. An excellent discussion from the point of view of the mixing-length theories has been given by Dryden (reference 20) and need not be repeated herein.

From equations (13) and (14), the local turbulent Prandtl number in terms of measurable quantities may be written as

$$\sigma_t = \frac{\overline{uv}}{\overline{\vartheta v}} \frac{\frac{\partial \theta}{\partial r}}{\frac{\partial U}{\partial r}} \tag{15}$$

or, in more convenient computational form,

$$\sigma_t = \frac{\left(\frac{\overline{uv}}{U_{max}^2}\right) \frac{\partial}{\partial r}\left(\frac{\theta}{\theta_{max}}\right)}{\left(\frac{\overline{\vartheta v}}{\theta_{max} U_{max}}\right) \frac{\partial}{\partial r}\left(\frac{U}{U_{max}}\right)} \tag{15a}$$

On the basis of the experimental results presented in the previous section, two different measures of σ_t can be computed: First, the effective turbulent Prandtl number for an entire section of the jet $\bar{\sigma}_t$ can be computed from a comparison between the width ratio of mean

velocity and temperature profiles in the turbulent jet and the same ratio as computed theoretically for a laminar jet. Second, the direct measurement of $\left(\frac{\overline{uv}}{U_{max}^2}\right)$ and $\left(\frac{\overline{\vartheta v}}{\theta_{max} U_{max}}\right)$ permits direct computation of the σ_t distribution, according to equation (15a). Of course, this latter result will not be very accurate, both because of the uncertainty of King's equation and because of the excessive experimental scatter.

Effective turbulent Prandtl number.- Effective turbulent Prandtl number provides another illustration of the usefulness of the integral equations when a complete solution is either not necessary or not feasible. For simplicity, the analysis is restricted to the constant-density case.

In addition to equations (4), (5), and (6), for the round jet an equation analogous in form to the mechanical-energy equation (2) can be derived by multiplying the heat-transfer equation by U before integration:

$$\frac{d}{dx}\int_0^\infty U^2\theta r\,dr = -\frac{1}{\rho c_p}\int_0^\infty rQ\frac{\partial U}{\partial r}\,dr - \frac{1}{\rho}\int_0^\infty r\tau\frac{\partial \theta}{\partial r}\,dr \qquad (16)$$

The physical significance of equation (16) is not so clear as that of equation (5). However, it may be regarded as a device for retaining Q (which disappears in the integration of the heat-transfer equation).

The solution for the velocity field of a laminar round jet has been given by Schlichting (reference 20) and by Bickley (reference 21), but the temperature field apparently has not been treated. For laminar flow,

$$\tau = \mu\frac{\partial U}{\partial r} \quad \text{and} \quad Q = k\frac{\partial \theta}{\partial r}$$

are substituted into equations (5) and (16), giving

$$\frac{d}{dx}\int_0^\infty U^3 r\,dr = -2\nu\int_0^\infty r\left(\frac{\partial U}{\partial r}\right)^2 dr \qquad (17)$$

and

$$\frac{d}{dx}\int_0^\infty U^2\theta r\,dr = -\nu\left(1+\frac{1}{\sigma}\right)\int_0^\infty r\,\frac{\partial U}{\partial r}\,\frac{\partial \theta}{\partial r}\,dr \tag{18}$$

It is to be expected that a good measure of the Prandtl number will be the difference in momentum and thermal diameters of the jet. The latter is defined so that

$$\frac{\pi\Delta_\theta^2}{4}\rho_{min}U_{max}\theta_{max} = 2\pi\int_0^\infty \rho U\theta r\,dr = N$$

Then equations (4) and (6) are replaced by the definition of Δ and the foregoing equation with ρ = Constant, that is,

$$U_{max}^2\Delta^2 = \frac{4M}{\pi\rho} \tag{19}$$

$$U_{max}\theta_{max}\Delta_\theta^2 = \frac{4N}{\pi\rho c_p} \tag{20}$$

With constant density, simple geometrical similarity exists, and there may be introduced the dimensionless variable $\eta' = \frac{2r}{\Delta}$, along with the functional assumptions $\frac{U}{U_{max}} = f(\eta')$ and $\frac{\theta}{\theta_{max}} = h(\eta')$.

Substitution of η' and f into equation (17), followed by substitution from equation (19) into the result, gives the differential equation

$$\frac{dU_{max}}{dx} = -2\pi\,\frac{I_2}{I_1}\,\frac{\mu}{M}\,U_{max}^2 \tag{21}$$

Substitution of η', f, and g into equation (18), followed by substitution from equation (20) into the result, gives the differential equation

$$\frac{dU_{max}}{dx} = -\pi \frac{I_4}{I_3} \frac{\mu c_p}{N} \left(1 + \frac{1}{\sigma}\right) U_{max}\theta_{max} \tag{22}$$

The I's are dimensionless integrals of f, g, and η'. Of course, equations (21) and (22) can be solved for $U_{max}(x)$ and $\theta_{max}(x)$, whence $\Delta(x)$ and $\Delta_\theta(x)$ are obtainable from equations (19) and (20). However, these results are not of primary interest herein.

Equating equation (21) to equation (22) gives

$$\frac{U_{max}}{\theta_{max}} = \frac{1}{2} \frac{I_1 I_4}{I_2 I_3} \frac{Mc_p}{N} \left(1 + \frac{1}{\sigma}\right) \tag{23}$$

Division of equation (20) by equation (19) gives

$$\frac{\Delta_\theta}{\Delta} = \left(\frac{N}{Mc_p} \frac{U_{max}}{\theta_{max}}\right)^{1/2}$$

which, with equation (23), yields

$$\frac{\Delta_\theta}{\Delta} = \left[\frac{1}{2}\left(1 + \frac{1}{\sigma}\right) \frac{I_1 I_4}{I_2 I_3}\right]^{1/2} \tag{24}$$

Without evaluating the I's individually, the product is obtained by considering as boundary condition the solution for $\sigma = 1$, which means that momentum and heat-transfer rates are identical. In this limiting case $\Delta_\theta = \Delta$, since the velocity and temperature distributions must be identical. Therefore, $\left(\frac{I_1 I_4}{I_2 I_3}\right) = 1$, and the final result is

$$\frac{\Delta_\theta}{\Delta} = \left[\frac{1}{2}\left(1 + \frac{1}{\sigma}\right)\right]^{1/2} \tag{25}$$

or, if this method is used to determine σ instead of to predict $\frac{\Delta_\theta}{\Delta}$,

$$\sigma = \frac{1}{2\left(\frac{\Delta_\theta}{\Delta}\right)^2 - 1} \tag{25a}$$

An identical treatment of a constant-density turbulent jet on the crude assumption of constant ϵ and β results, of course, in

$$\bar{\sigma}_t = \frac{1}{2\left(\frac{\Delta_\theta}{\Delta}\right)^2 - 1} \tag{26}$$

where $\bar{\sigma}_t$ is the over-all effective Prandtl number for the turbulent-jet cross section.

For air, in the normal range of room temperature, the considerable scatter in thermal conductivities obtained in the various experimental determinations leads to an approximate range of possible true (laminar) Prandtl numbers, $0.70 \leq \sigma \leq 0.76$. A tabular and graphical summary of "best" measured values up to 1938 has been made by Tribus and Boelter (reference 23). They give, for example, $\sigma = 0.708$ for $\bar{T}_a = 302^\circ$ abs. and 0.701 for $\bar{T}_a = 348^\circ$ abs. These particular values have been chosen for comparison with two computations of the turbulent measurements.

For the present turbulent jet, at $\frac{x}{d} = 15$ and initial temperature differences of $\bar{\theta}_o = 15^\circ$ C and 300° C, the width ratios are $\frac{\Delta_\theta}{\Delta} = 1.102$ and 1.107, respectively. From equation (26), these give $\bar{\sigma}_t = 0.701$ and 0.690. With the two orifice temperatures given, the average absolute temperatures across the section are about 302° abs. and 348° abs. (these numbers are actually $\bar{T}_r + \frac{1}{2}\bar{\theta}_{max}$). This gives the extremely interesting result that the average of effective turbulent Prandtl number in a round jet is equal to the laminar value, within the probable accuracy of the present measurements.

Turbulent Prandtl number distribution.- Faired curves for the measurements of $\frac{\overline{uv}}{\bar{U}_{max}^2}$ and $\frac{\overline{\vartheta v}}{\bar{\theta}_{max}\bar{U}_{max}}$ (fig. 25) have been used, along

with the dimensionless velocity and temperature profiles, to compute local values of σ_t, in accordance with equation (15a). The values have been plotted in figure 27, along with a heavy line giving $\bar{\sigma}_t$ as computed from $\frac{\Delta\theta}{\Delta}$. Near the axis and near the jet edge, the computation becomes more or less indeterminate.

The agreement between $\bar{\sigma}_t$ and the average value of the σ_t points is extremely good. In fact, it is rather better than was anticipated, because of the considerable scatter of the fluctuation measurements and the possible inexactness of King's equation.

DISCUSSION

Errors

Most of the sources of error and the corrections, both applied and not applied, have been covered in the previous sections. However, it may be well to outline and extend the previous remarks.

Total-head-tube and thermocouple data.- The total-head-tube readings have not been corrected for the effect of velocity and density fluctuations (appendix A). Also, since the range of possible sensitivities was quite limited and since the response is proportional to $\bar{U}^2$, the deflections near the jet edge were small and difficult to obtain accurately.

A certain amount of experimental scatter in all measured quantities resulted from small fluctuations in $\bar{U}_o$, due primarily to the partly stalled condition of the blower, which was designed to operate against a somewhat smaller pressure rise.

The temperature distributions for small $\bar{\theta}_o$ and at large $\frac{x}{d}$ and $\frac{r}{r_1}$ were naturally susceptible to considerable scatter due to slow temperature fluctuations of perhaps a fraction of a degree in the laboratory.

Hot-wire measurements.- The usual sources of error (see discussions by Dryden (reference 23) and Simmons (reference 24)) for hot-wire measurements were encountered in the present investigation.

Two additional difficulties were attributable to the particular flow configuration: First, the extremely high turbulence level present in a free jet is certainly outside of the small disturbance assumptions basic to the standard hot-wire response calculations. However, some rather brief measurements (reference 12) indicate that opposite errors may reduce this error considerably. Second, the extremely large degree of fluctuation introduces some uncertainty in the bridge balancing for the setting of hot-wire resistance.

The principal additional source of error inherent in the hot-jet measurements was the extreme difficulty of determining $\overline{R}_a$, the unheated wire resistance at local ambient temperature $\overline{T}_a$. Since the ϑ' sensitivity of a wire is proportional to $\overline{R}_a - R_r$ (where R_r is the unheated resistance at T_r), it is clear that, in regions of relatively small $\overline{\theta}$, a small error in $\overline{R}_a$ may cause a large error in $\frac{\vartheta'}{\overline{\theta}}$, and as it turns out, also in $\frac{\overline{\vartheta u}}{\overline{\theta U}}$. The complexity of the computational procedures in these new applications of the hot-wire anemometer, often involving small differences between two large quantities, each with a fairly large amount of experimental scatter, has obviously magnified this scatter immensely in the final results.

Because of the foregoing factors, it was felt that hot-wire length corrections were not appropriate; the scale of the turbulence was of the order of 0.5 to 1 centimeter, and the scale of temperature fluctuations was probably of the same order of magnitude.

However, it should be emphasized that free jet measurements represent the most stringent kind of test for the new measuring technique. It is certain that similar investigations in channels and boundary layers, for example, will show more consistent experimental points.

Variation of Jet Spread with Density

As pointed out, the considerable divergence between computed and measured curves of $\frac{\Delta}{\Delta_1}$ against $\frac{\rho_\infty}{\rho_o}$ (fig. 15) is probably due to the very rough nature of the simplifying assumption used. Apparently the curve shapes agree reasonably well. This theoretical curve is computed particularly for the case in which density difference is obtained by heating; the relation between heat and momentum transfer determines the relation between the velocity function $f(\eta)$ and the density function $g(\eta)$ and thus determines the ratio $\frac{I_2}{I_1}$ in equation (12). In cases where the density difference is obtained by the use of different gases, $\frac{I_2}{I_1}$ may be different, so that the curve of $\frac{\Delta}{\Delta_1}$ against $\frac{\rho_\infty}{\rho_o}$ will not be the same. However, it does not seem likely that material diffusion in turbulent shear flow is much different from momentum and heat diffusion,[2] so the final result should be fairly close to that computed herein.

---

[2]At the Seventh International Congress for Applied Mechanics, B. G. van der Hegge Zijnen and J. O. Hinze reported careful measurements showing heat and material diffusion to be effectively the same in a round turbulent jet.

Fluctuation Levels

There are two characteristics of the measured fluctuation levels that are worthy of note. The first is that $\frac{u'}{\overline{U}} > \frac{\vartheta'}{\overline{\theta}}$ everywhere in the jet. Although there must be some uncertainty since the complete physical form of King's equation has never been verified (appendix A, reference 16), the fact that $\frac{u'}{\overline{U}}$ in the heated jet is measured at about the same value as in the cold jet seems evidence that the results are reasonable. An additional bit of evidence is the result that $\frac{\vartheta'}{\overline{\theta}_{max}} > \frac{u'}{\overline{U}_{max}}$ in the outer part of the jet $\left(\text{where } \frac{\partial}{\partial r}\left(\frac{\overline{\theta}}{\overline{\theta}_{max}}\right) > \frac{\partial}{\partial r}\left(\frac{\overline{U}}{\overline{U}_{max}}\right)\right)$, whereas $\frac{u'}{\overline{U}_{max}} > \frac{\vartheta'}{\overline{\theta}_{max}}$ near the axis $\left(\text{where } \frac{\partial}{\partial r}\left(\frac{\overline{U}}{\overline{U}_{max}}\right) > \frac{\partial}{\partial r}\left(\frac{\overline{\theta}}{\overline{\theta}_{max}}\right)\right)$. This is quite consistent with the result arrived at by the conventional qualitative phenomenological approach which considers a u fluctuation (or a ϑ fluctuation) arising from a v fluctuation with a fixed mixing length. Thus, if this (purely fictitious, but sometimes convenient) mixing length were about the same for velocity and temperature fluctuations, u' would be relatively greater than ϑ' where the $\overline{U}$ profile was relatively steeper than the $\overline{\theta}$ profile, and vice-versa. Of course, this does not necessarily account for the slight local minimum in $\frac{\vartheta'}{\overline{\theta}_{max}}$ on the jet axis.

Relative Transfer of Heat and Momentum

The σ_t distribution shown in figure 27, although agreeing in average with $\overline{\sigma}_t$ computed directly from $\frac{\Delta_\theta}{\Delta}$, does not necessarily prove any significant result with regard to the function $\sigma_t(r)$. Both the experimental scatter in the $\overline{uv}$ and $\overline{\vartheta v}$ measurements and the difficulty of making accurate slope determinations from the mean velocity and temperature profiles permit only the conclusion that σ_t is roughly constant across the main part of a round turbulent jet.

That the effective turbulent Prandtl number might possibly be the same as the laminar Prandtl number was apparently first suggested by Dryden (reference 19), though not with any particular physical justification. In fact, it appears that no one has yet put forth any rational hypothesis, either rigorous or phenomenological, to predict the relative rates of heat and momentum transfer in turbulent shear flow.

Since the vorticity transport theory is apparently the only analytical approach that has led even to the qualitatively correct result, it seems probable that simple momentum-exchange considerations will be inadequate.

SUMMARY OF RESULTS

From measurements of mean total-head and temperature fields in a round turbulent jet with various initial temperatures, the following enumerated results can be stated with confidence:

1. The rate of spread of a round turbulent jet increases with a decrease in the density of jet fluid relative to receiving medium. When the density difference is obtained by heating, the effect is as shown by the experimental points in figure 15.

2. Up to a local maximum density ratio ρ_∞/ρ_{min} of about 1.3 simple geometrical similarity still exists in a fully developed jet, within the accuracy of the present measurements. The total-head and temperature profile functions are effectively the same as in the constant-density jet.

3. The average or effective "turbulent Prandtl number," for a section in the fully developed jet, is very nearly equal to the laminar Prandtl number.

4. The local turbulent Prandtl number at a section in the fully developed jet, away from axis and edge, is roughly constant. In addition, with somewhat less certainty, it has been found that $\frac{\vartheta'}{\bar{\theta}} < \frac{u'}{\bar{U}}$ everywhere in the jet and that the relative magnitude of $\frac{\vartheta'}{\bar{\theta}_{max}}$ and $\frac{u'}{\bar{U}_{max}}$ varies roughly as the relative magnitude of the slopes of dimensionless temperature and velocity profiles.

California Institute of Technology
Pasadena, Calif., August 18, 1947

APPENDIX A

EFFECT OF SIMULTANEOUS VELOCITY AND DENSITY FLUCTUATIONS ON READING OF A TOTAL-HEAD TUBE

Neglecting both static-pressure fluctuations and the effect of lateral velocity fluctuations, the tube reading is

$$P = \frac{1}{2}\overline{(\bar{\rho} + \rho')(\bar{U} + u)^2} \tag{A1}$$

Therefore, since $\overline{\bar{\rho}\bar{U}u} = 0$,

$$P = \frac{1}{2}\bar{\rho}\left(\bar{U}^2 + \overline{u^2}\right) + \bar{U}\overline{\rho' u} + \frac{1}{2}\overline{\rho' u^2} \tag{A2}$$

For small fluctuations the last term can be neglected. Also, since the density fluctuations of interest herein are due to temperature fluctuations,

$$\rho' = -\bar{\rho}\frac{\vartheta}{\bar{T}_a}$$

is substituted into equation (A2), which finally gives for the true mean dynamic pressure in terms of the tube reading:

$$\frac{1}{2}\bar{\rho}\bar{U}^2 = \frac{P}{1 + \dfrac{\overline{u^2}}{\bar{U}^2} - \dfrac{\bar{\theta}}{\bar{T}_a}\left(\dfrac{\overline{\vartheta u}}{\bar{\theta}\bar{U}}\right)} \tag{A3}$$

It is interesting to note that, since $\overline{\vartheta u}$ is apparently ordinarily positive, the errors due to the velocity and the temperature fluctuations are in opposite directions.

The justification for neglecting the effect of lateral fluctuations in this approximate calculation is that its effect on the magnitude of the instantaneous velocity vector is at least partially balanced by the directional sensitivity of the tube.

REFERENCES

1. Pabst, O.: Die Ausbreitung Heisser Gasstrahlen in Bewegter Luft. Untersuchungen und Mitteilungen Nr. 8004, Aug. 1944.

2. Pabst, O., and Von Bohl, J. G.: Mischungsvorgang eines Leuchtgasstrahles mit Ruhender Luft. FW-Hausbericht 09 021 I.

3. Hu, N.: On the Turbulent Mixing of Two Fluids of Different Densities. Part II of Ph.D. Thesis, C.I.T., 1944.

4. Goff, J. A., and Coogan, C. H.: Some Two-Dimensional Aspects of the Ejector Problem. Jour. Appl. Mech., vol. 9, no. 4, Dec. 1942, pp. A-151 - A-154.

5. Abramovich, G. N.: The Theory of a Free Jet of a Compressible Gas. NACA TM No. 1058, 1944.

6. Liepmann, Hans Wolfgang, and Laufer, John: Investigations of Free Turbulent Mixing. NACA TN No. 1257, 1947.

7. Ribner, Herbert S.: Field of Flow about a Jet and Effect of Jets on Stability of Jet-Propelled Airplanes. NACA ACR No. L6C13, 1946.

8. Squire, H. B., and Trouncer, J.: Round Jets in a General Stream. R. & M. No. 1974, British A.R.C., 1944.

9. Liepmann, H. W., Corrsin, S., and Laufer, J.: Some Measurements in Free Turbulent Shear Flow. Note presented at Sixth Int. Cong. for Appl. Mech., Sept. 1946.

10. Ruden, P.: Turbulente Ausbreitungsvorgänge im Freistrahl. Die Naturwissenschaften, Jahrg. 21, Heft 21/23, May 26, 1933, pp. 375-378.

11. Kuethe, Arnold M.: Investigations of the Turbulent Mixing Regions Formed by Jets. Jour. Appl. Mech., vol. 2, no. 3, Sept. 1935, pp. A-87 - A-95.

12. Corrsin, Stanley: Investigation of Flow in an Axially Symmetrical Heated Jet of Air. NACA ACR No. 3L23, 1943.

13. Goldstein, S., ed.: Modern Developments in Fluid Dynamics. Vol. II. Clarendon Press (Oxford), 1938, pp. 672-673.

14. Howarth, L.: Concerning the Velocity and Temperature Distributions in Plane and Axially Symmetrical Jets. Proc. Cambridge Phil. Soc., vol. 34, 1938, pp. 185-203.

15. Corrsin, Stanley: Extended Applications of the Hot-Wire Anemometer. The Rev. Sci. Instr., vol. 18, no. 7, July 1947, pp. 469-471.

16. Corrsin, S.: Extended Applications of the Hot-Wire Anemometer. NACA TN No. 1864, 1949.

17. King, Louis Vessot: On the Convection of Heat from Small Cylinders in a Stream of Fluid: Determination of the Convection Constants of Small Platinum Wires with Applications to Hot-Wire Anemometry. Phil. Trans. Roy. Soc. (London), ser. A, vol. 214, 1914, pp. 373-432.

18. Bowen, W. H.: Tests of Axial Flow Fans Designed by Lattice Theory. M.S. Thesis, C.I.T., 1938.

19. Dryden, H. L.: Aerodynamics of Cooling. Vol. VI of Aerodynamic Theory, div. T, W. F. Durand, ed., Julius Springer (Berlin), 1934.

20. Schlichting, H.: Laminare Strahlausbreitung. Z.f.a.M.M., Bd. XIII, 1933, pp. 260-263.

21. Bickley, W. G.: The Plane Jet. Phil. Mag., vol. 23, April 1937.

22. Tribus, Myron, and Boelter, L. M. K.: An Investigation of Aircraft Heaters. II - Properties of Gases. NACA ARR, Oct. 1942.

23. Dryden, Hugh L.: Isotropic Turbulence in Theory and Experiment. Theodore von Kármán Anniversary Volume, C.I.T. (Pasadena), 1941.

24. Simmons, L. F. G.: Note on Errors Arising in Measurements of Turbulence. R. & M. No. 1919, British A.R.C., 1939.

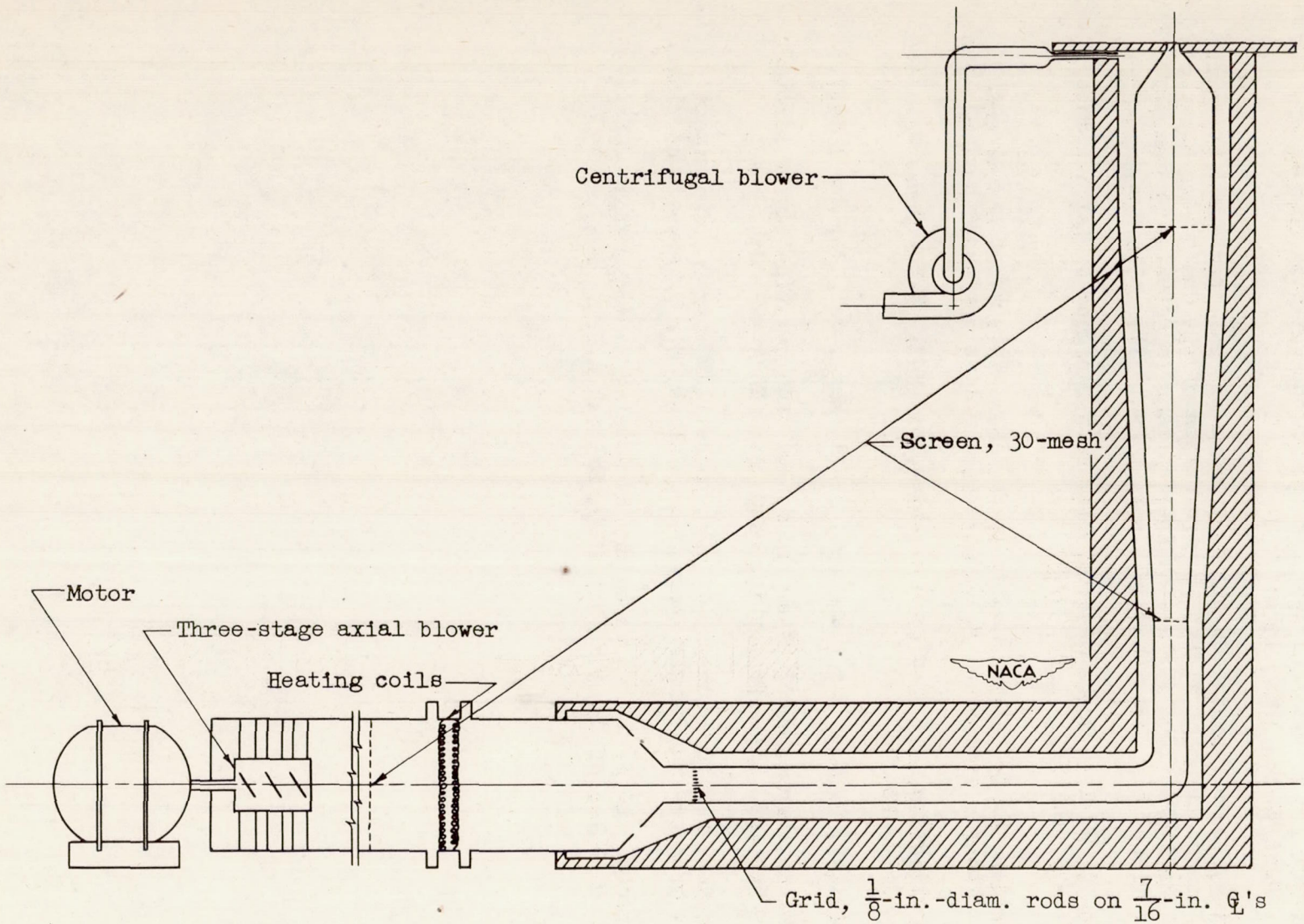

Figure 1.- Schematic presentation of 1-inch heated jet. Approximately one-eighth full size.

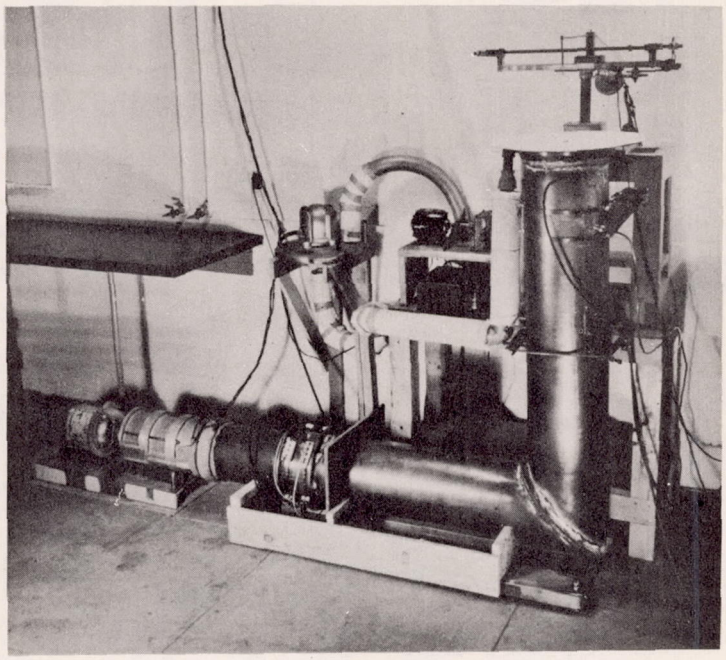

(a) Complete hot-jet unit.

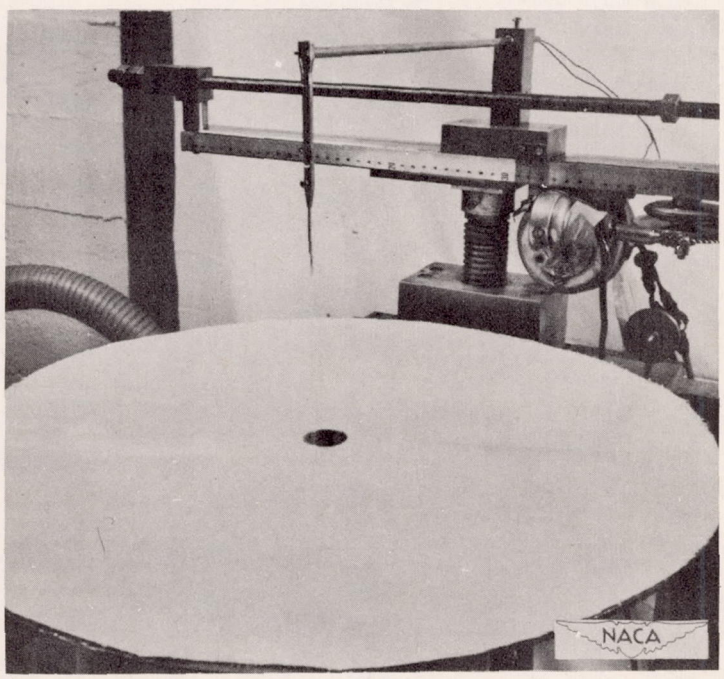

(b) Close-up of orifice and traverse track.

Figure 2.- Test setup.

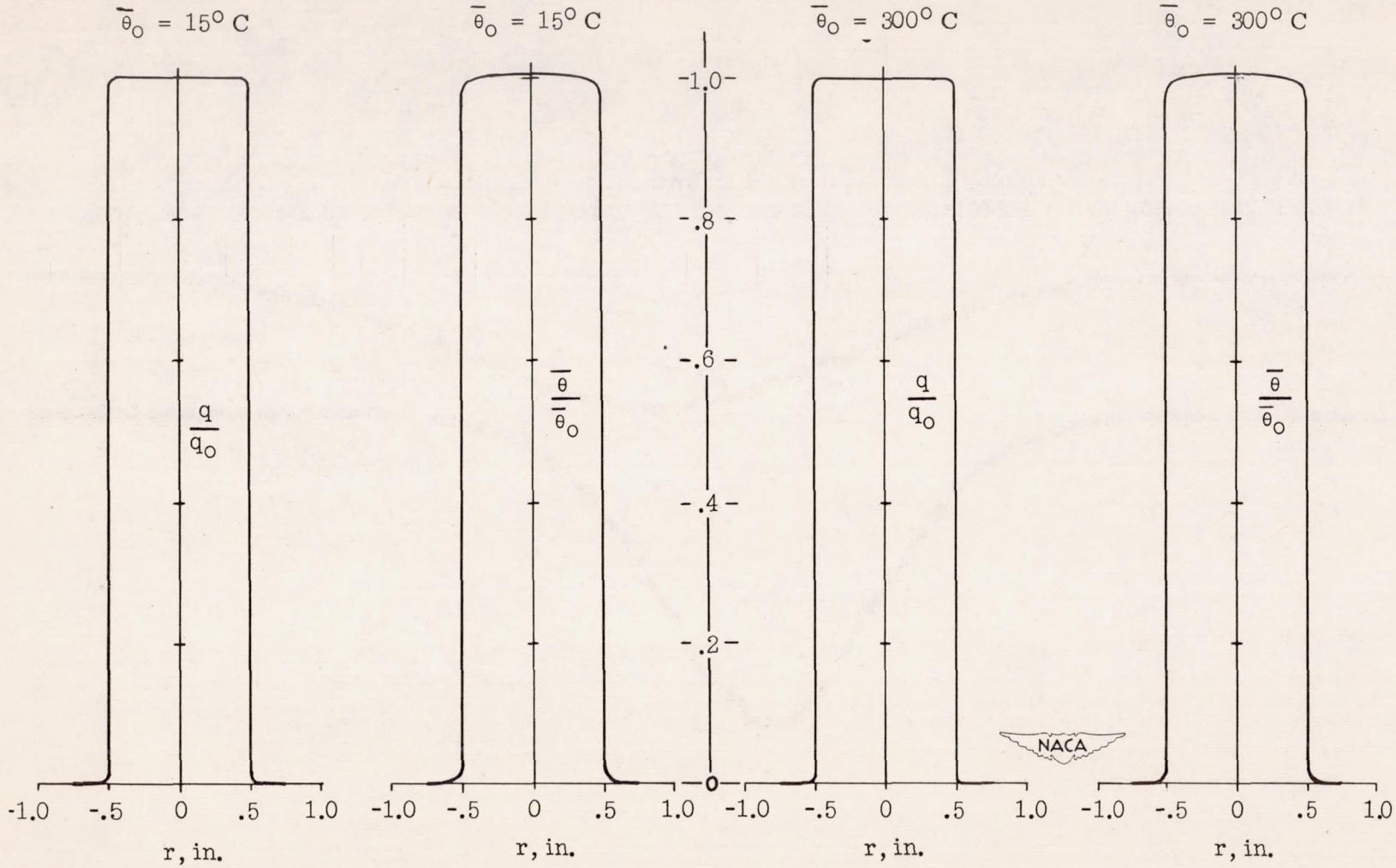

Figure 3.- Initial temperature and total-head distributions. 1-inch round jet. q_o = 40 millimeters of alcohol.

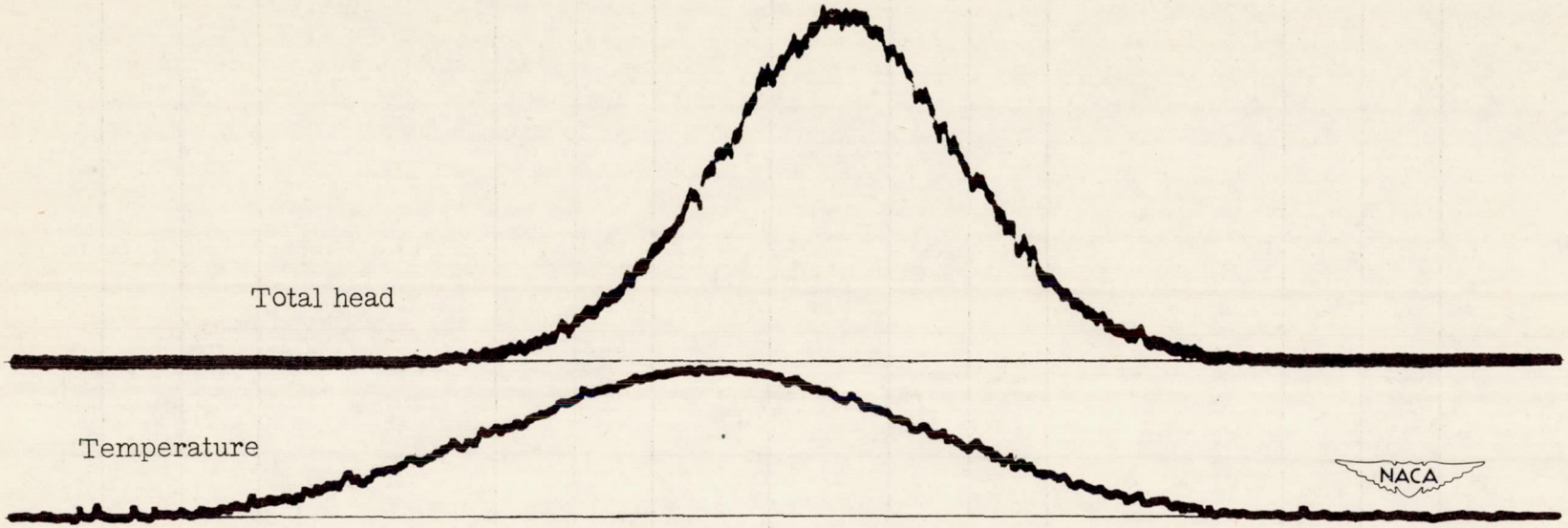

Figure 4.- Sample photographic record of mean total head and temperature. 1-inch heated jet. Lateral offset of records is due to instrument spacing.

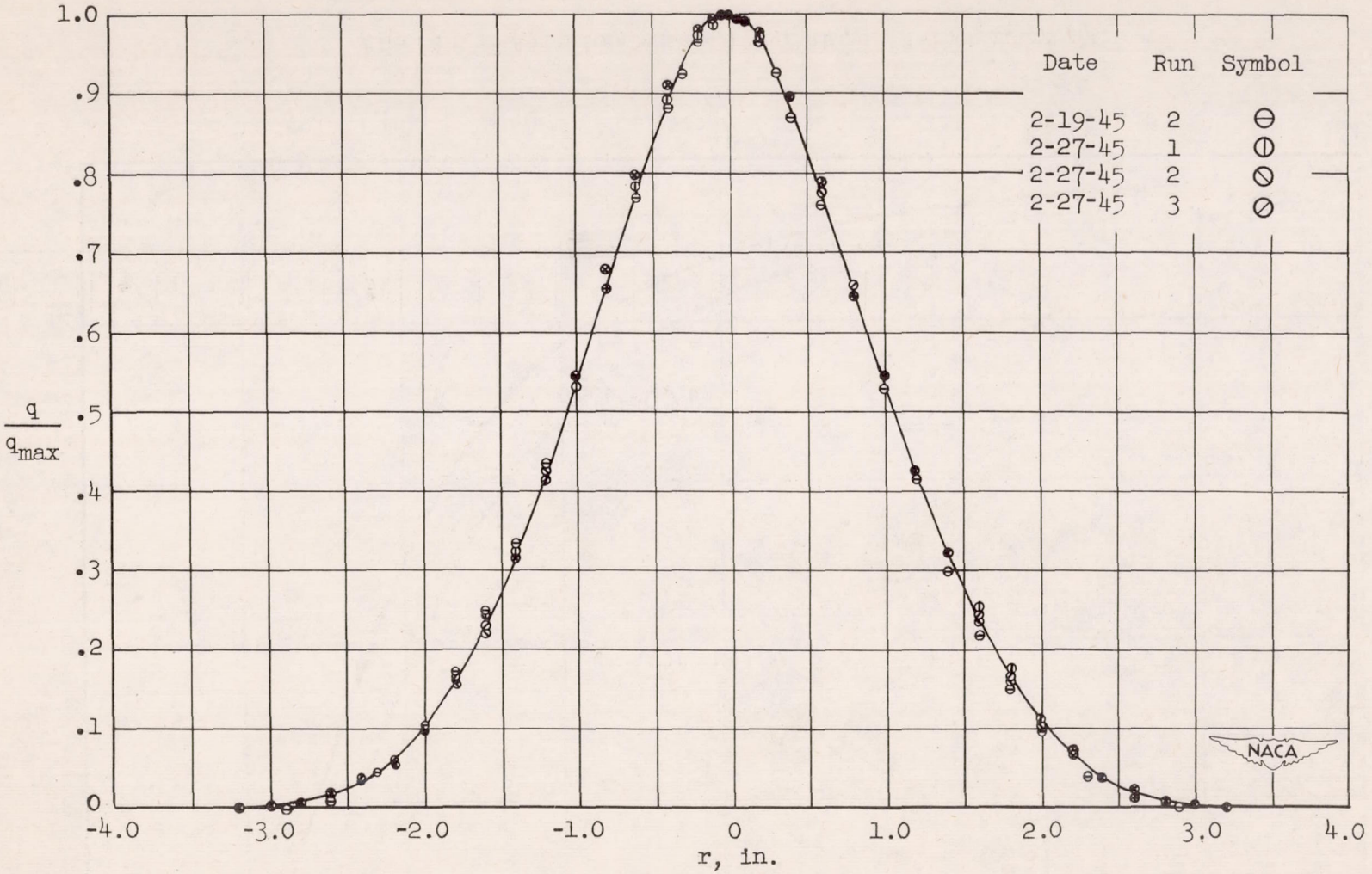

Figure 5.- Experimental scatter. 1-inch heated jet. x = 15 inches; $\theta_o = 280^\circ$ C.

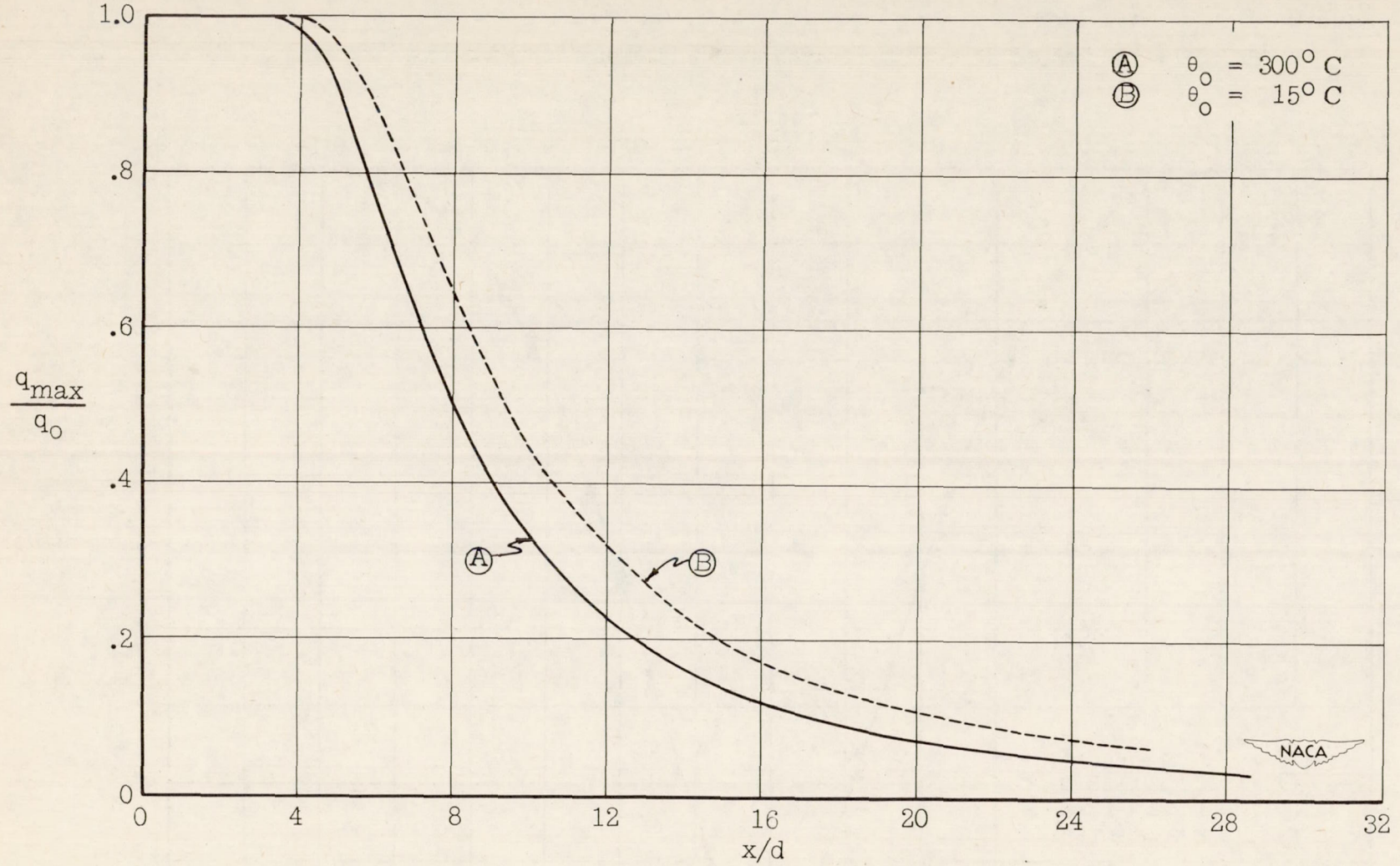

Figure 6.- Axial total-head distributions. 1-inch round jet.

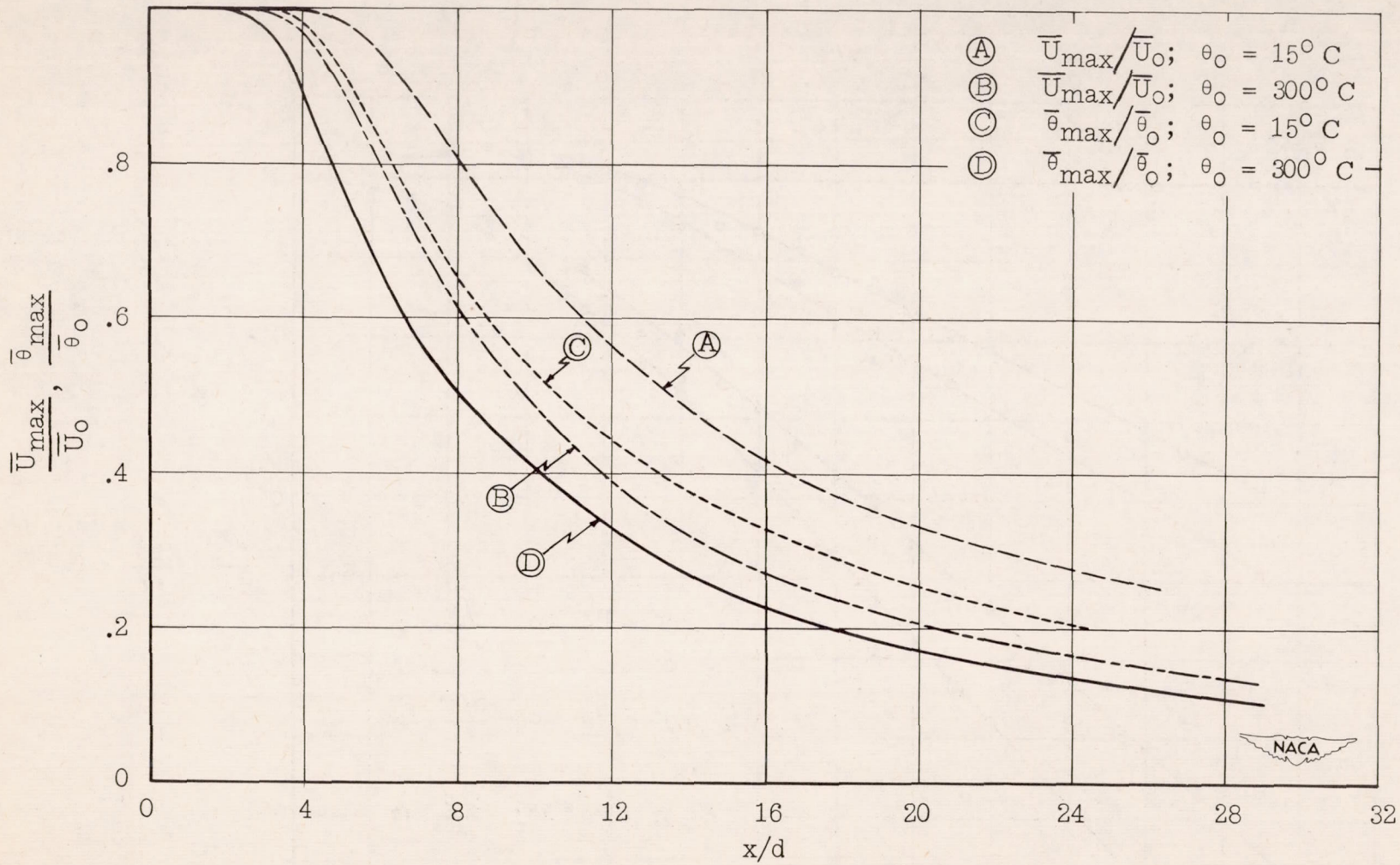

Figure 7.- Axial velocity and temperature distributions. 1-inch round jet.

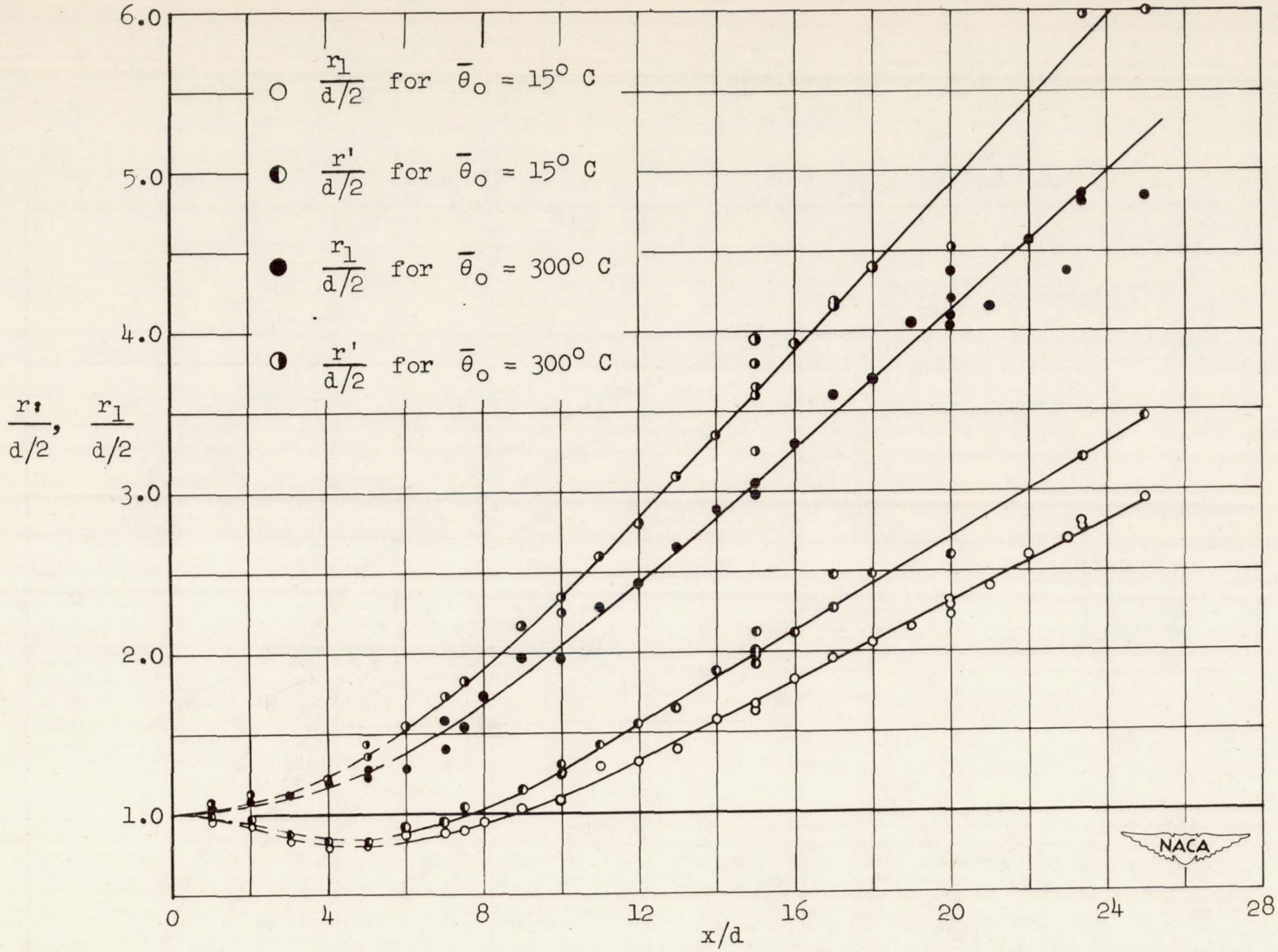

Figure 8.- Spread of heat and momentum. 1-inch round jet.

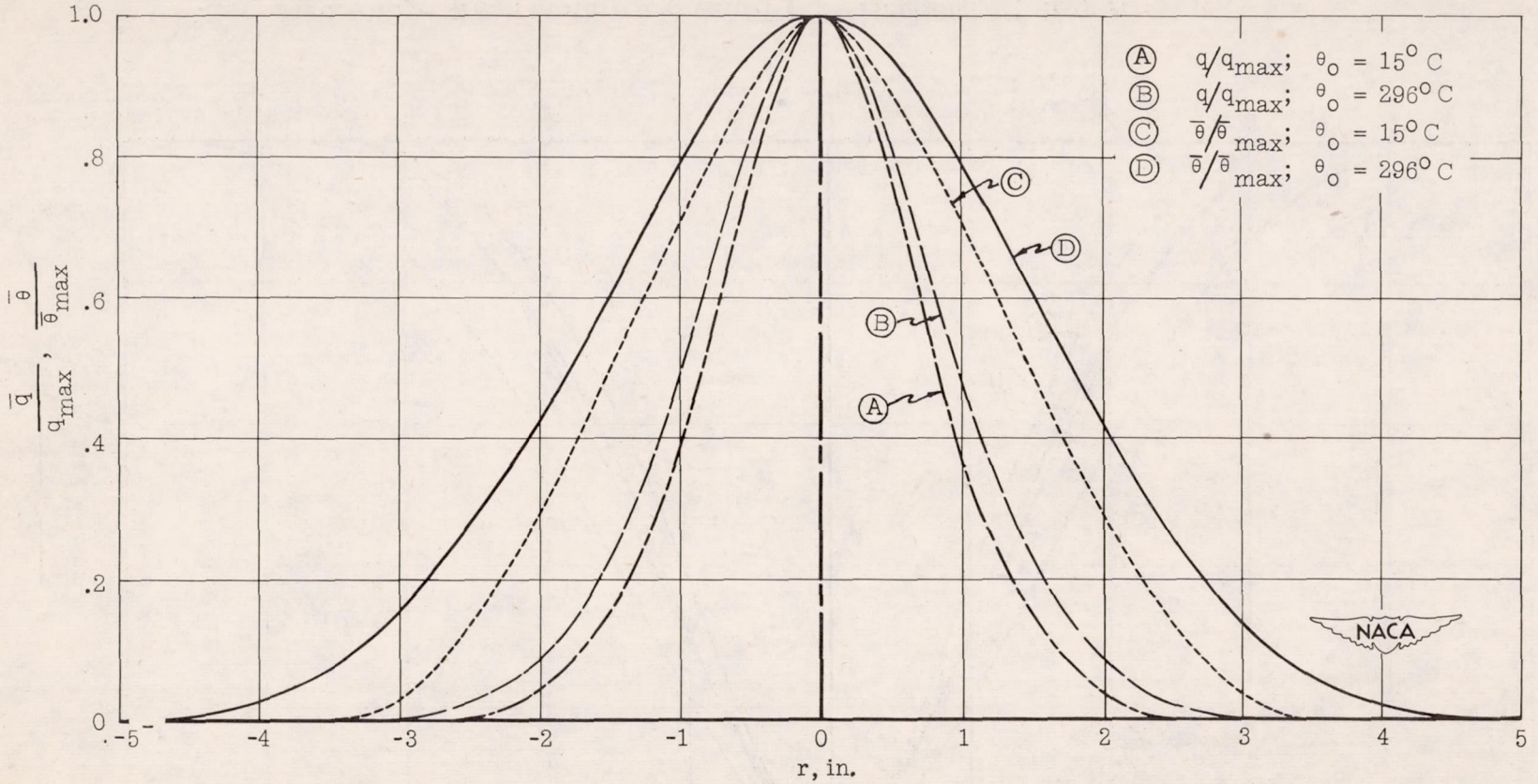

Figure 9.- Total-head and temperature distributions. 1-inch round jet. $\frac{x}{d}$ = 15.

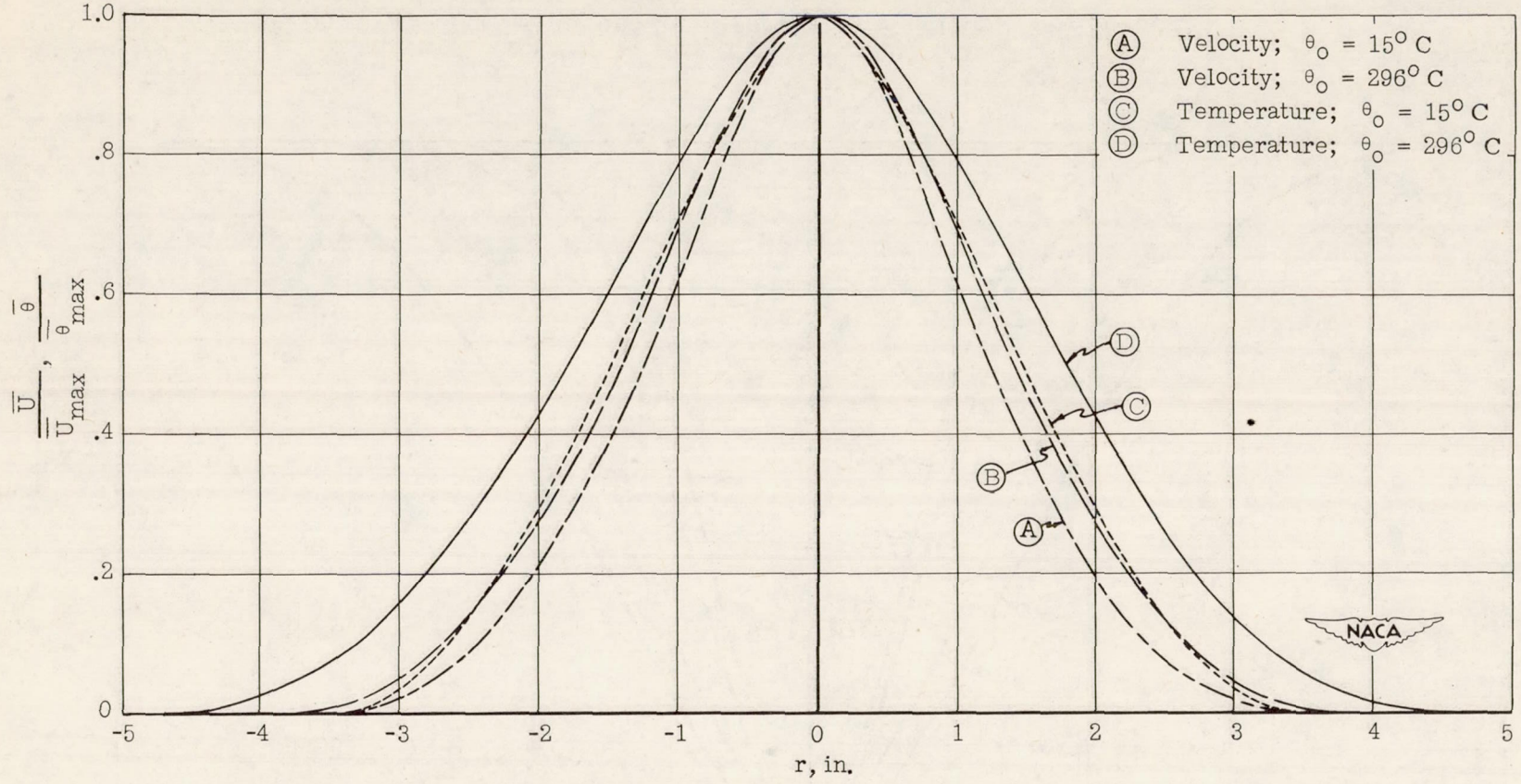

Figure 10.- Temperature and velocity distributions. 1-inch round jet. $\frac{x}{d}$ = 15.

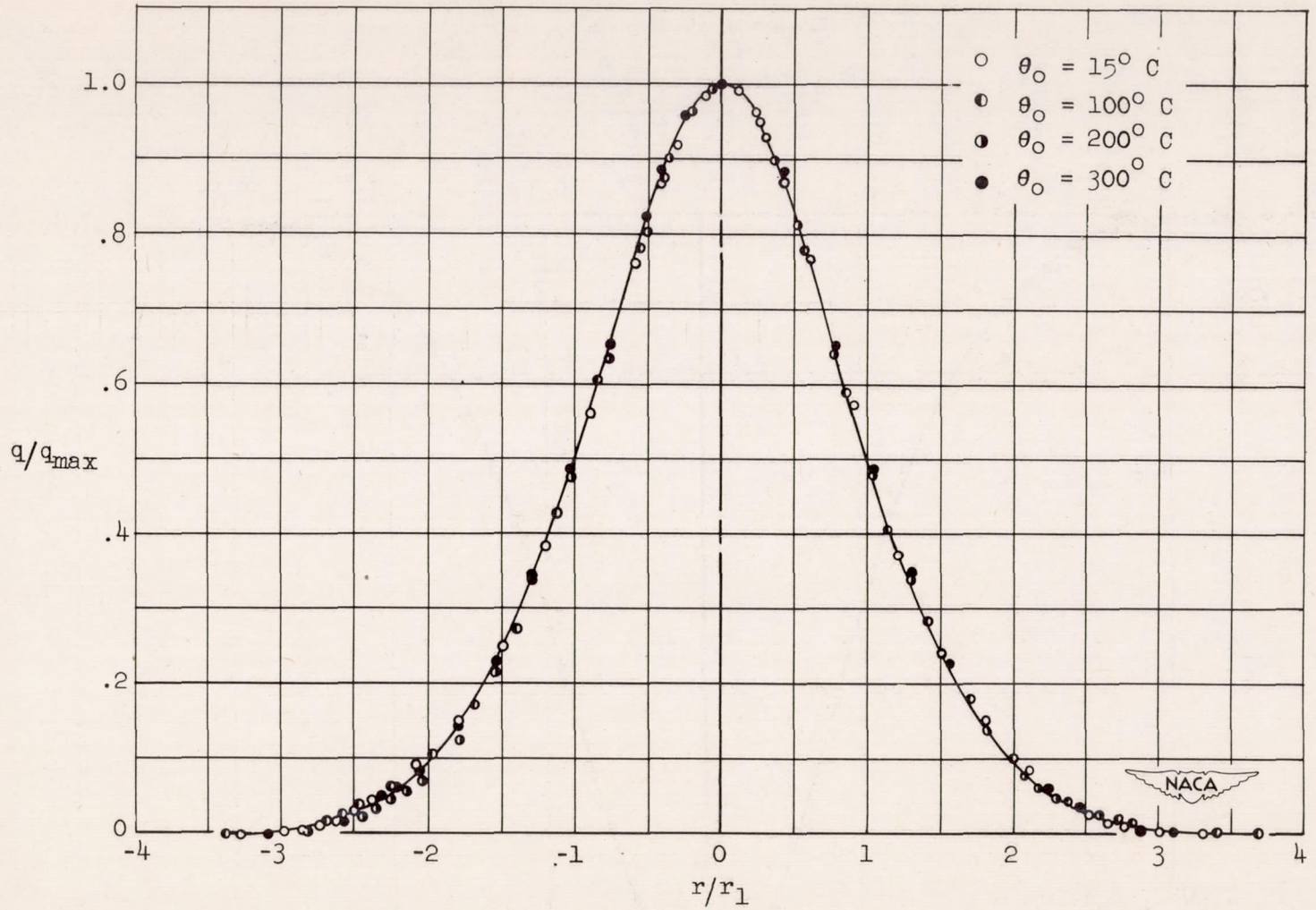

Figure 11.- Check on similarity of total-head distribution. 1-inch hot jet. $\frac{x}{d} = 15$; $r_1 = r$ at which $q = \frac{1}{2} q_{max}$.

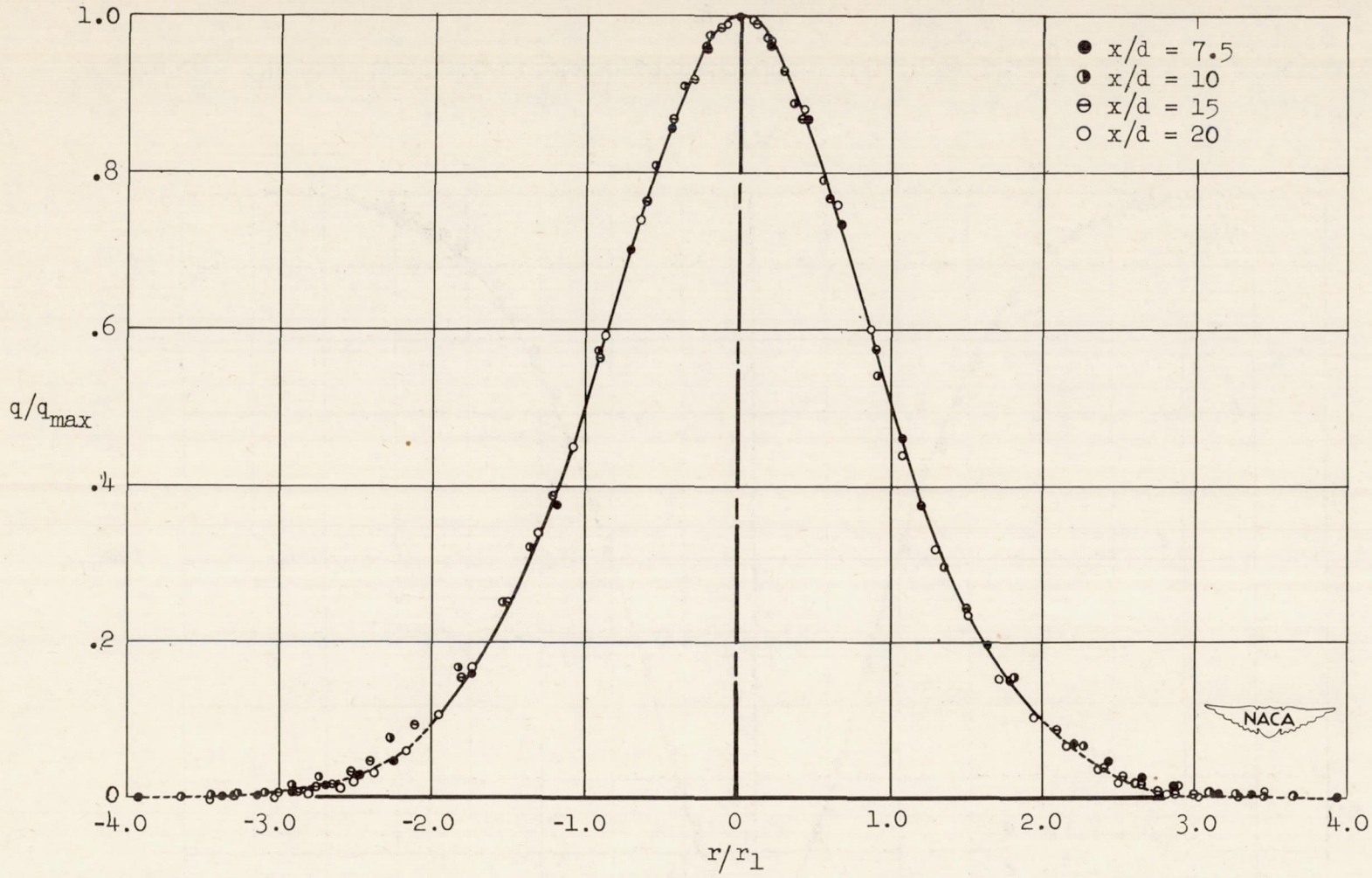

Figure 12.- Check on similarity of total-head distributions. Constant-density jet. $\tilde{\theta}_o = 15^o$ C. $r_1 = r$ at which $q = \frac{1}{2} q_{max}$.

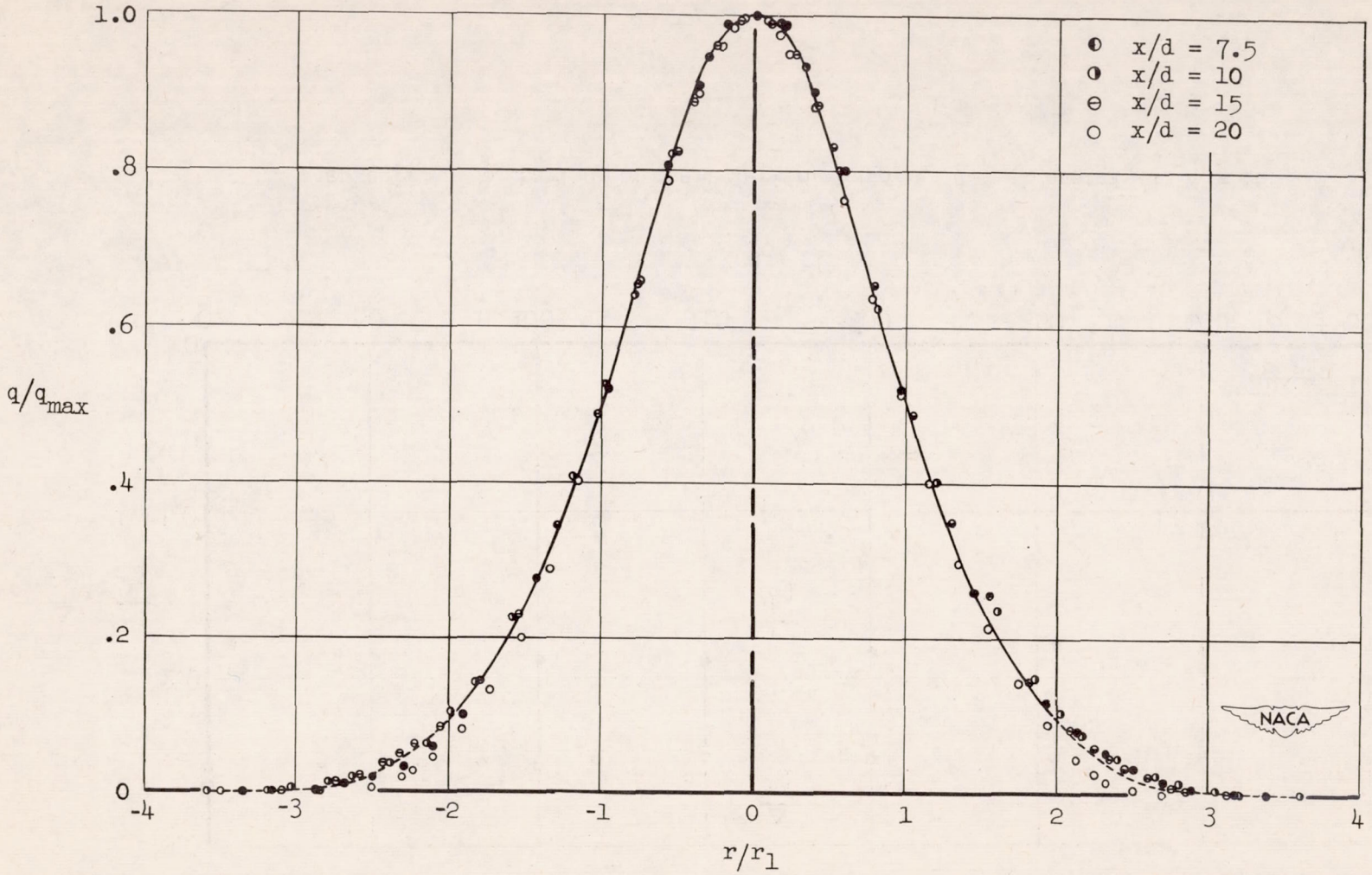

Figure 13.- Check on similarity of total-head distributions. 1-inch hot jet. $\overline{\theta}_o = 300^\circ$ C. $r_1 = r$ at which $q = \frac{1}{2} q_{max}$.

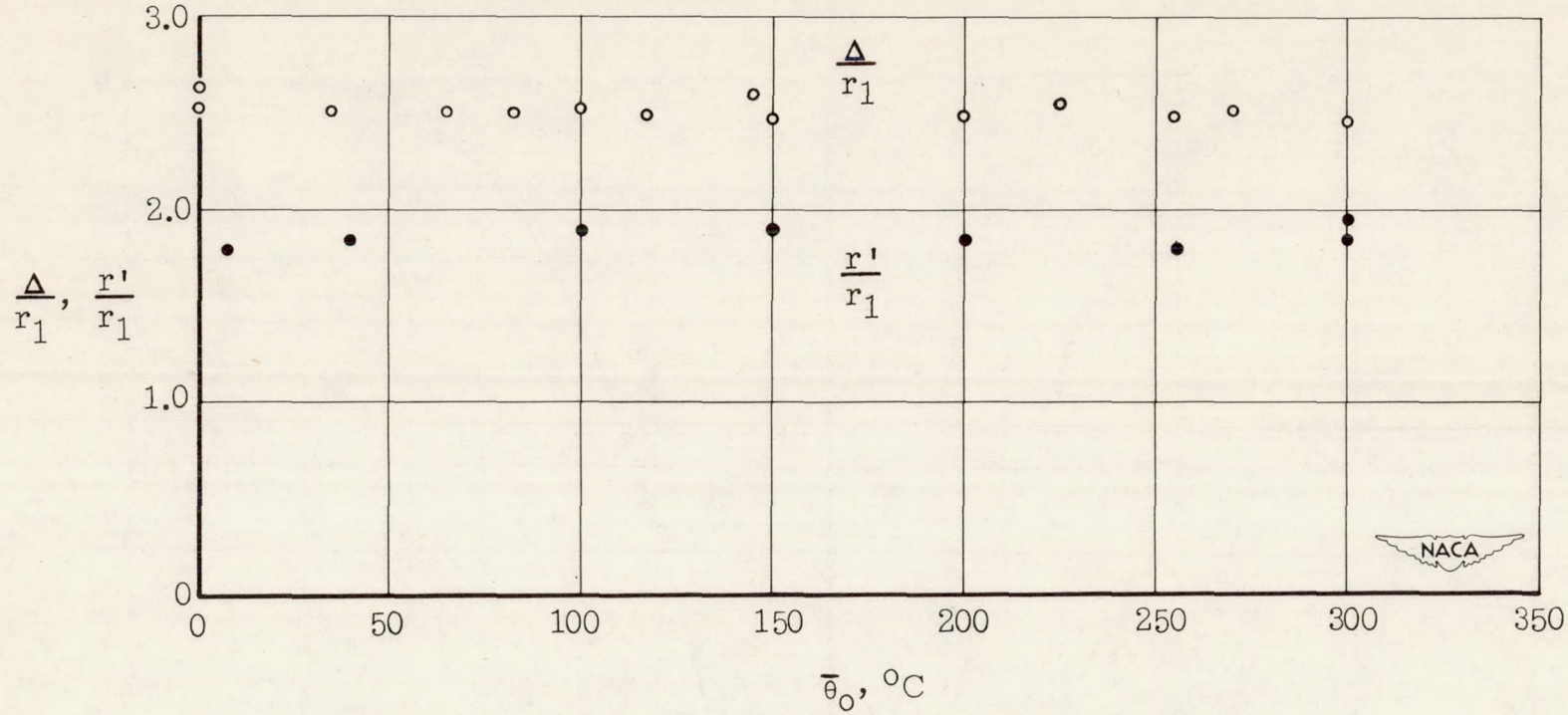

Figure 14.- Comparison of characteristic lengths. 1-inch heated jet. $\frac{x}{d} = 15$.

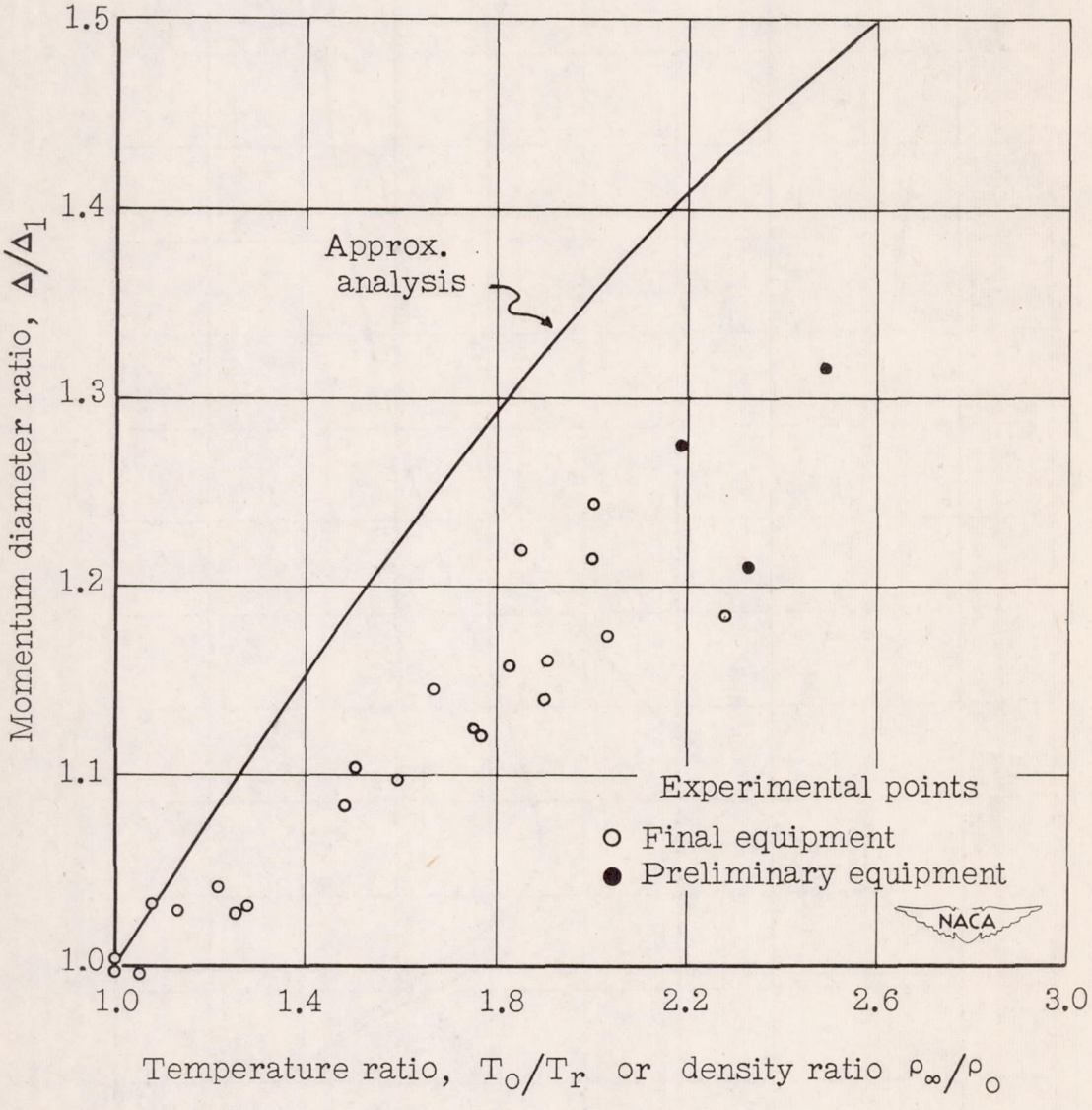

Figure 15.- Variation of momentum diameter with initial temperature or density ratio. Hot jet. $\frac{x}{d} = 15$.

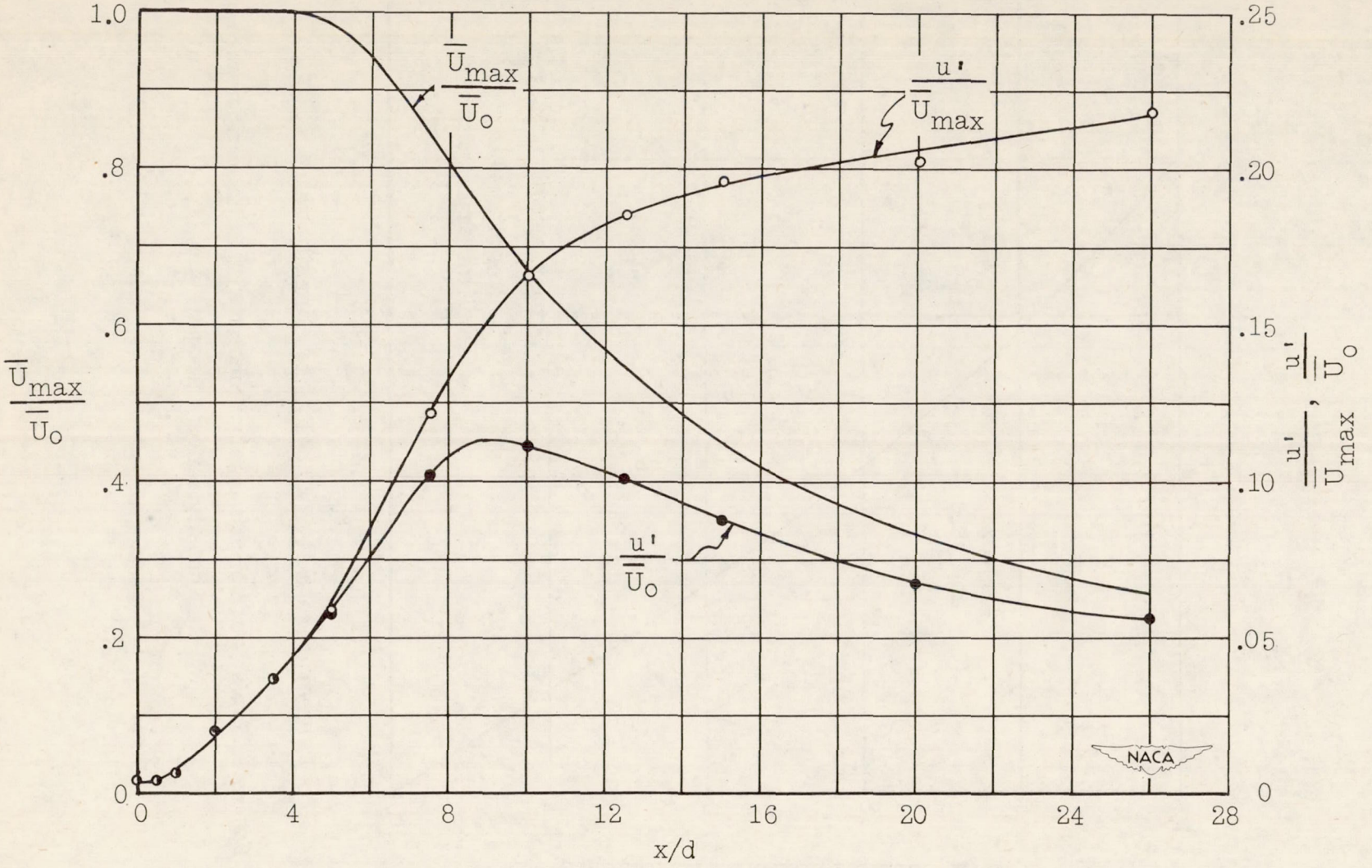

Figure 16.- Axial velocity fluctuation levels. 1-inch round jet. $\overline{\theta}_o = 15^\circ$ C.

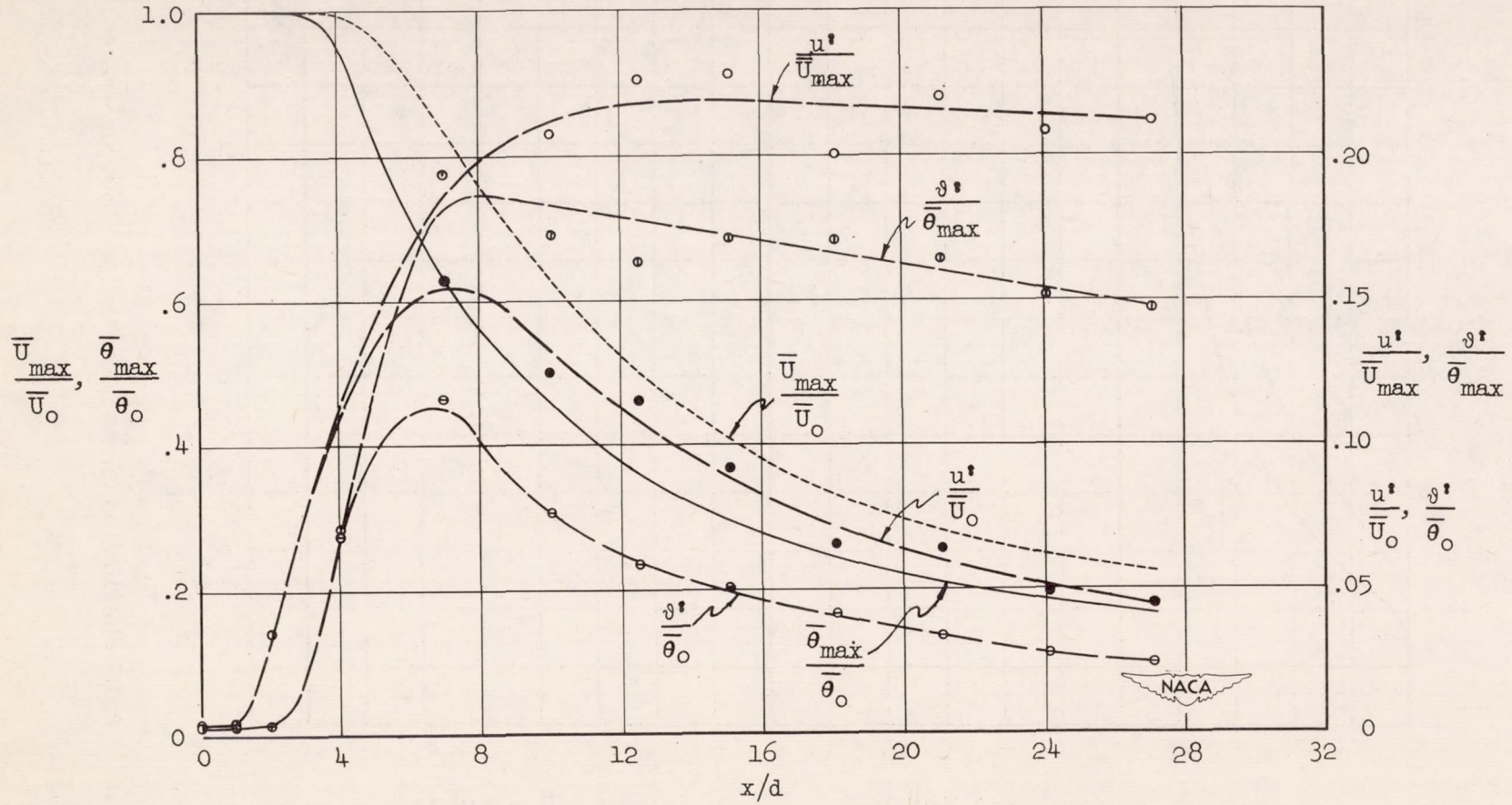

Figure 17.- Axial distribution of fluctuations. 1-inch hot jet. $\overline{\theta}_o = 170^o$ C.

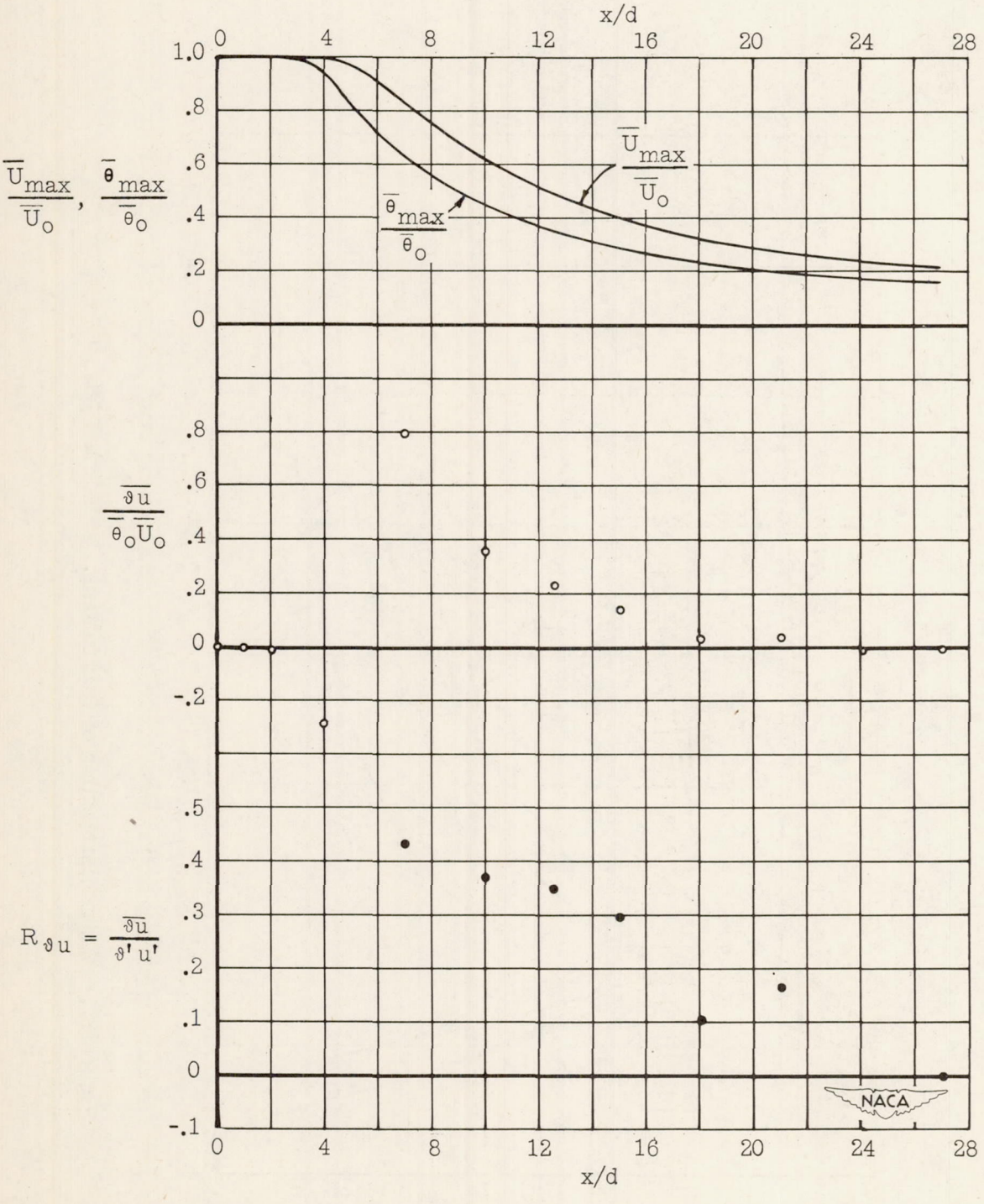

Figure 18.- Axial distribution of $\overline{\vartheta u}$ correlation. Hot jet. $\overline{\theta}_o = 170^\circ$ C.

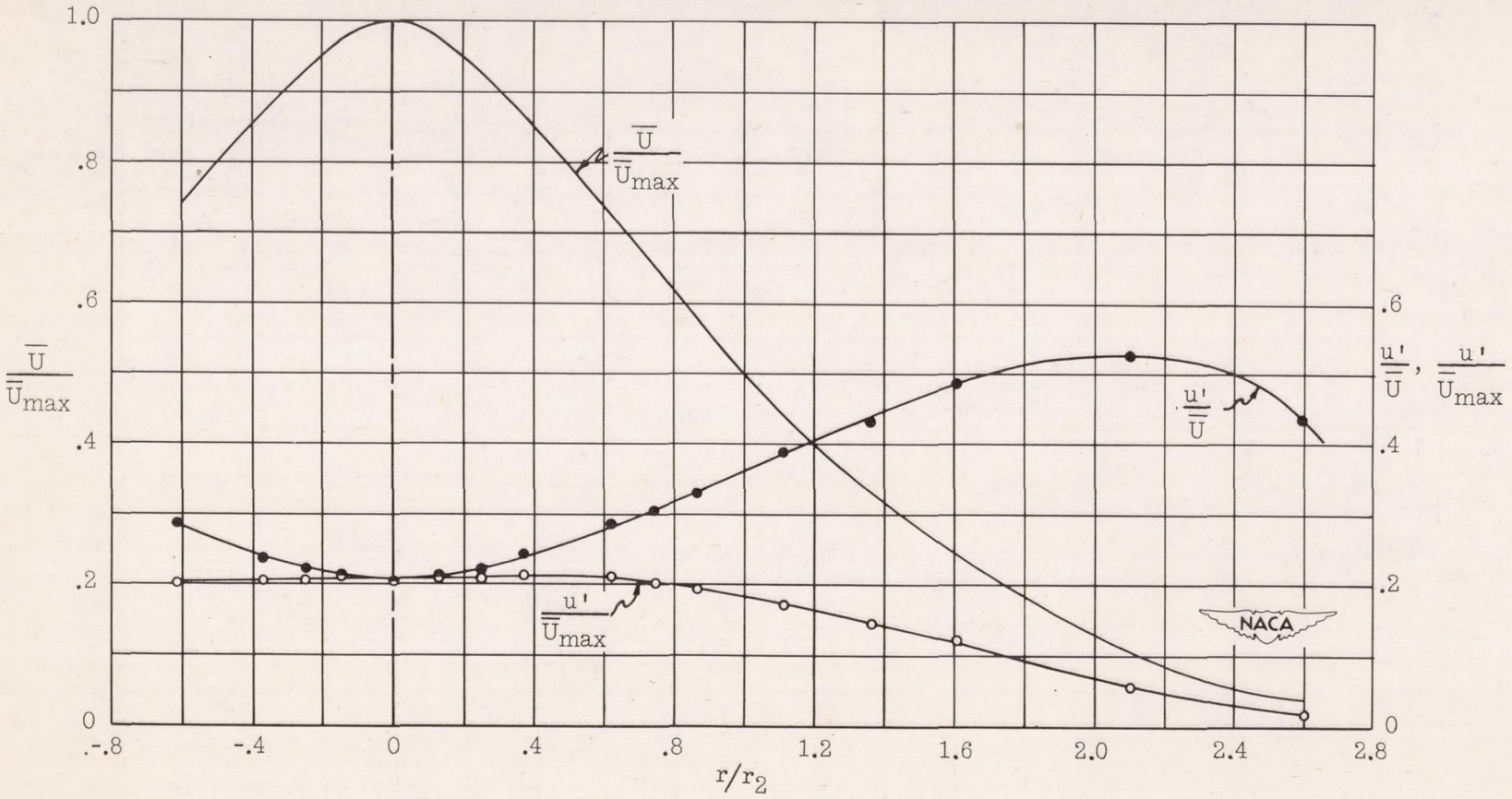

Figure 19.- Check measurement of lateral u' distribution. Cold jet. $\frac{x}{d} = 20$.

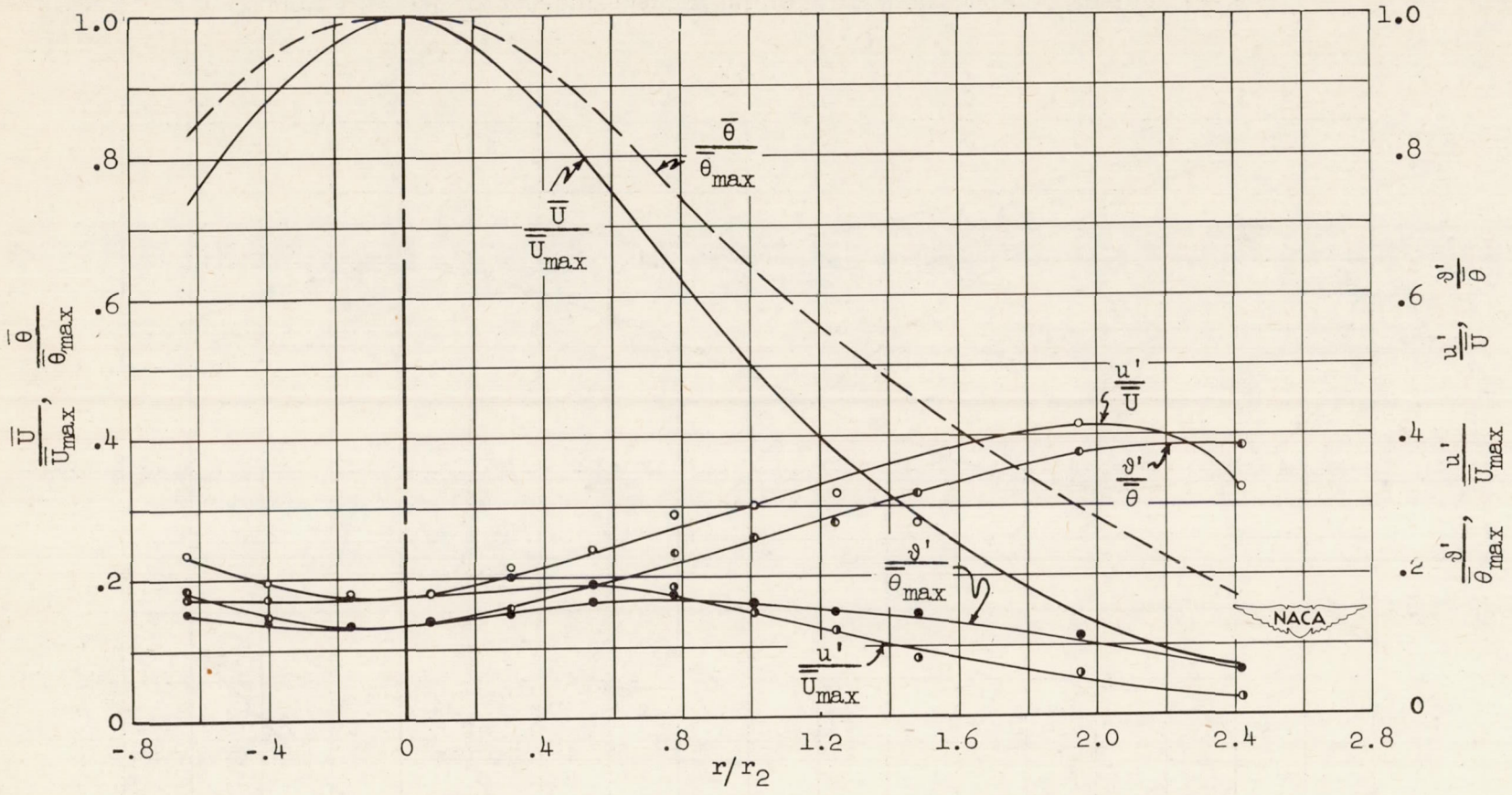

Figure 20.- Fluctuation levels. Hot jet. $\frac{x}{d} = 20$; $\bar{\theta}_o = 170^\circ$ C.

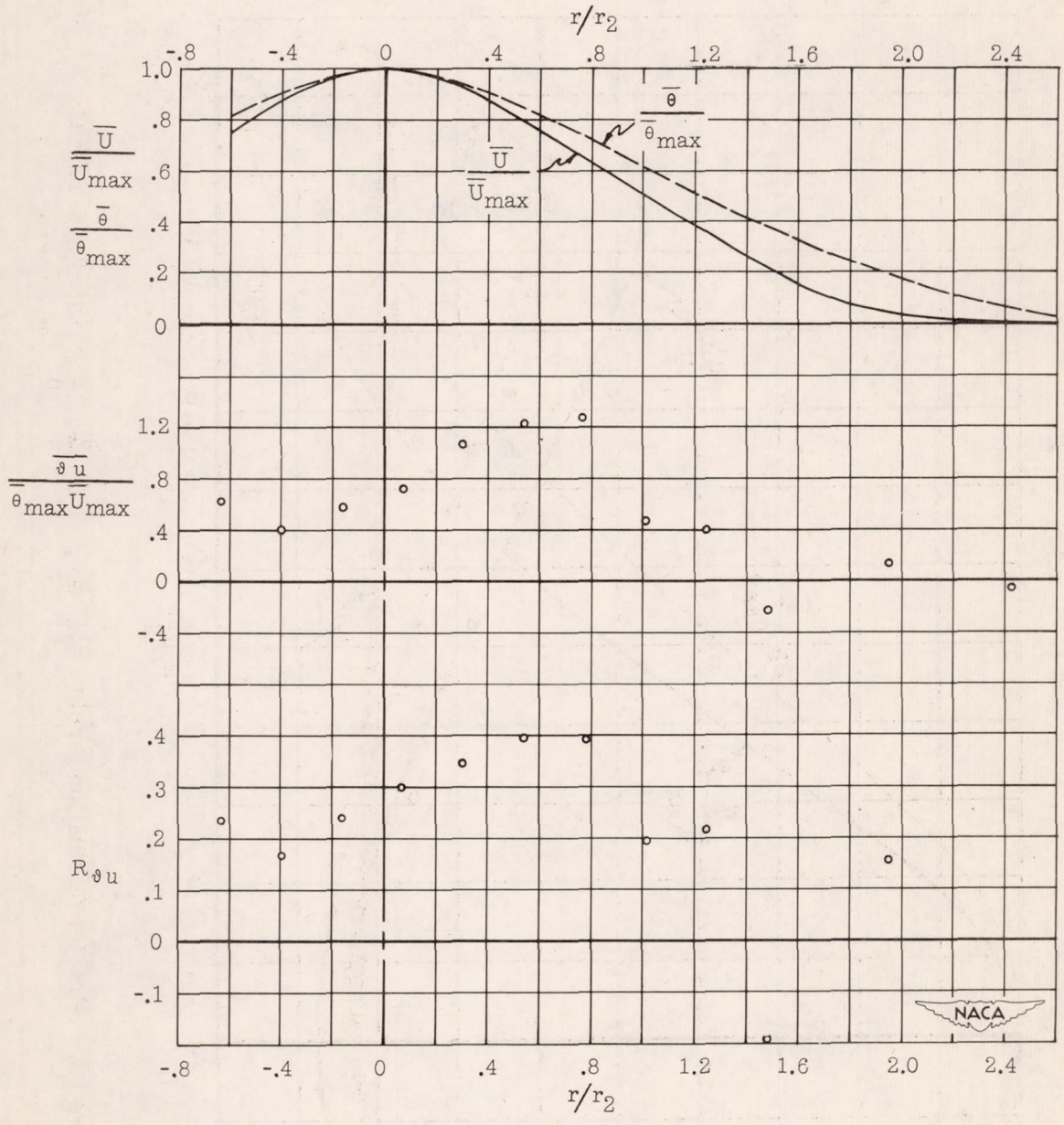

Figure 21.- The $\overline{\vartheta u}$ correlation. Hot jet. $\frac{x}{d} = 20$; $\overline{\theta}_o = 170^\circ$ C.

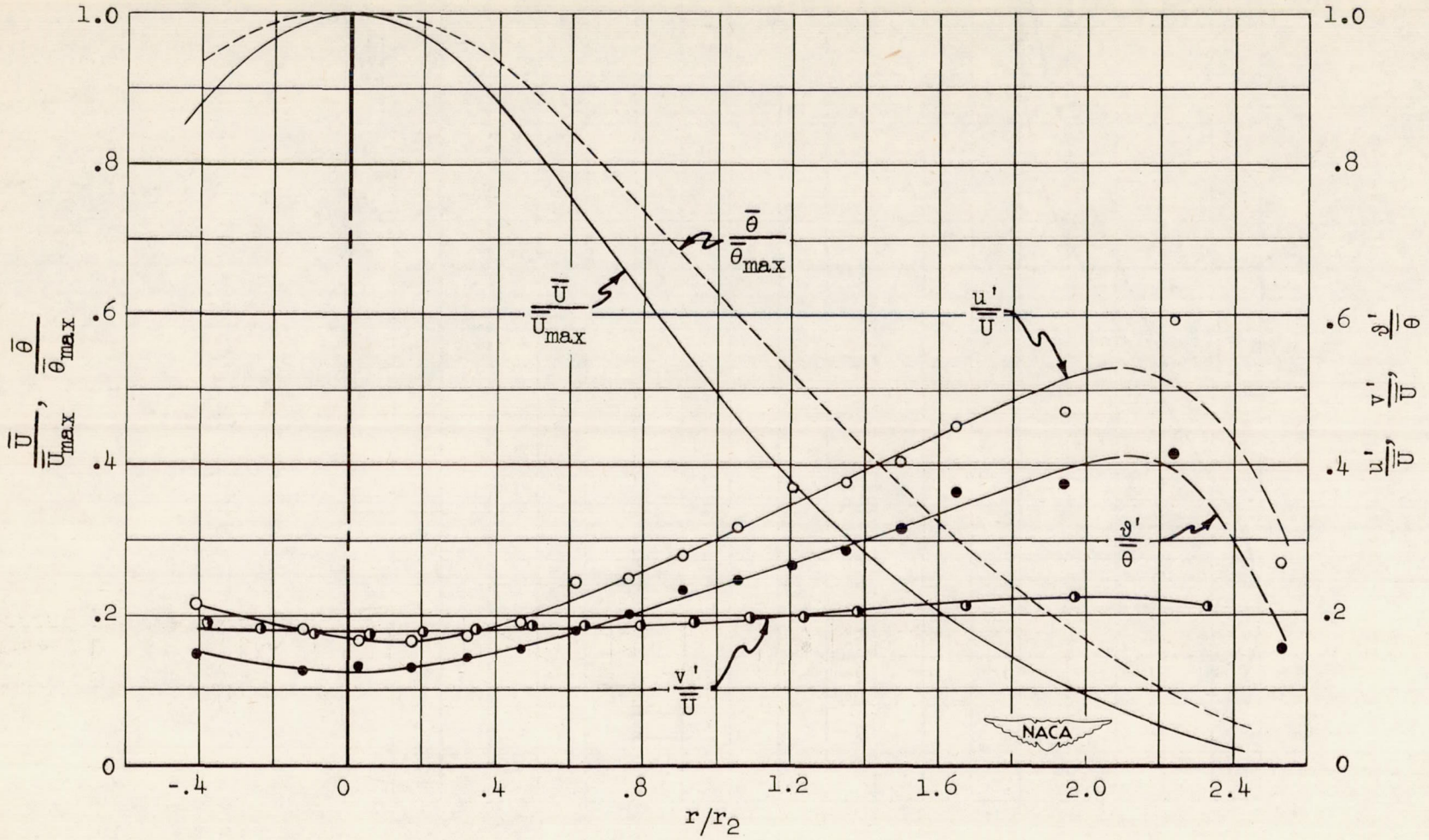

Figure 22.- Hot-jet fluctuation levels $\frac{u'}{\bar{U}}$, $\frac{v'}{\bar{U}}$, and $\frac{\vartheta'}{\bar{\theta}}$. $\frac{x}{d} = 15$; $\bar{\theta}_o = 170^\circ$ C.

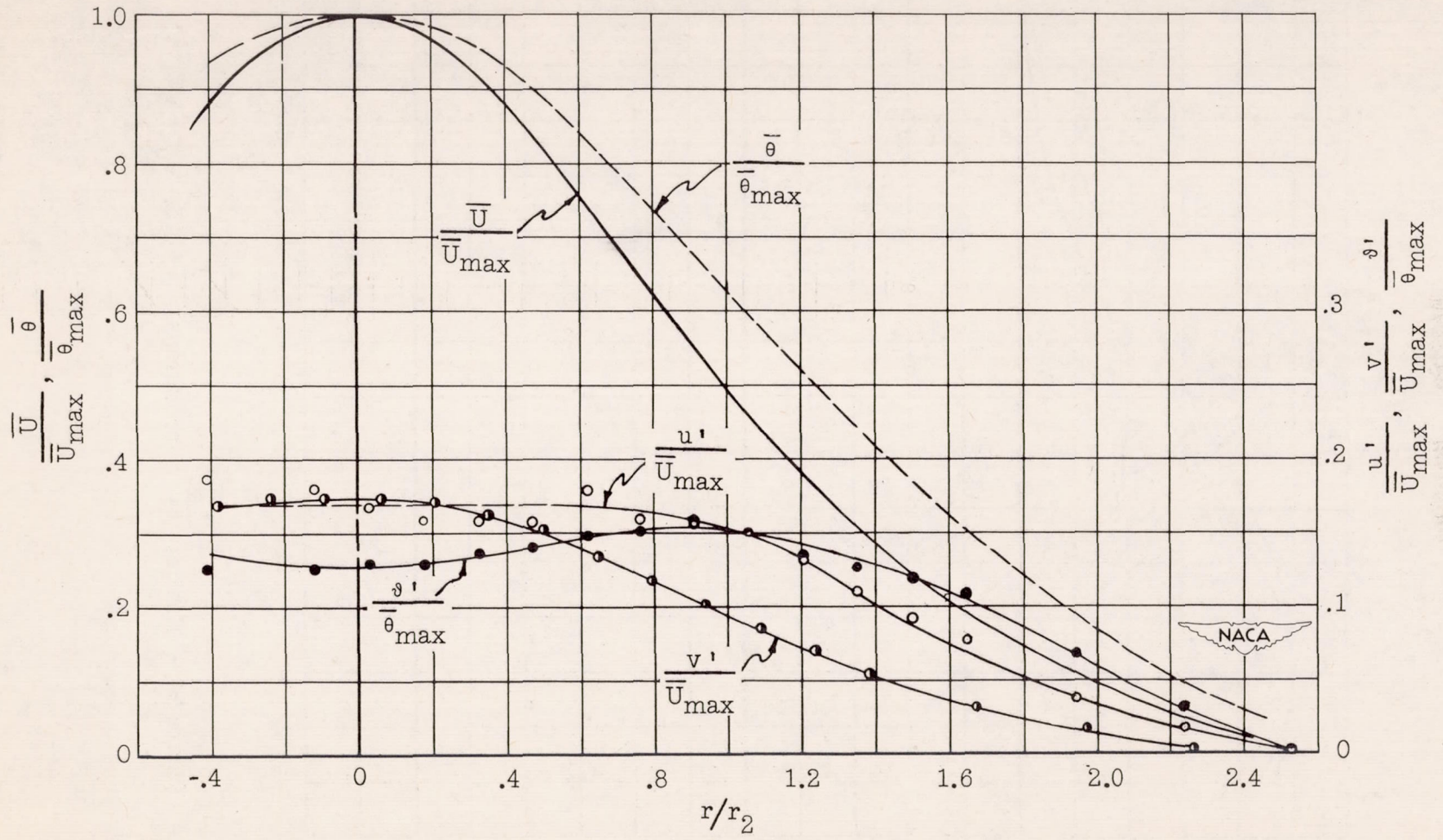

Figure 23.- Hot-jet fluctuation levels $\frac{u'}{\bar{U}_{max}}$, $\frac{v'}{\bar{U}_{max}}$, and $\frac{\vartheta'}{\bar{\theta}_{max}}$. $\frac{x}{d} = 15$; $\bar{\theta}_o = 170^\circ$ C.

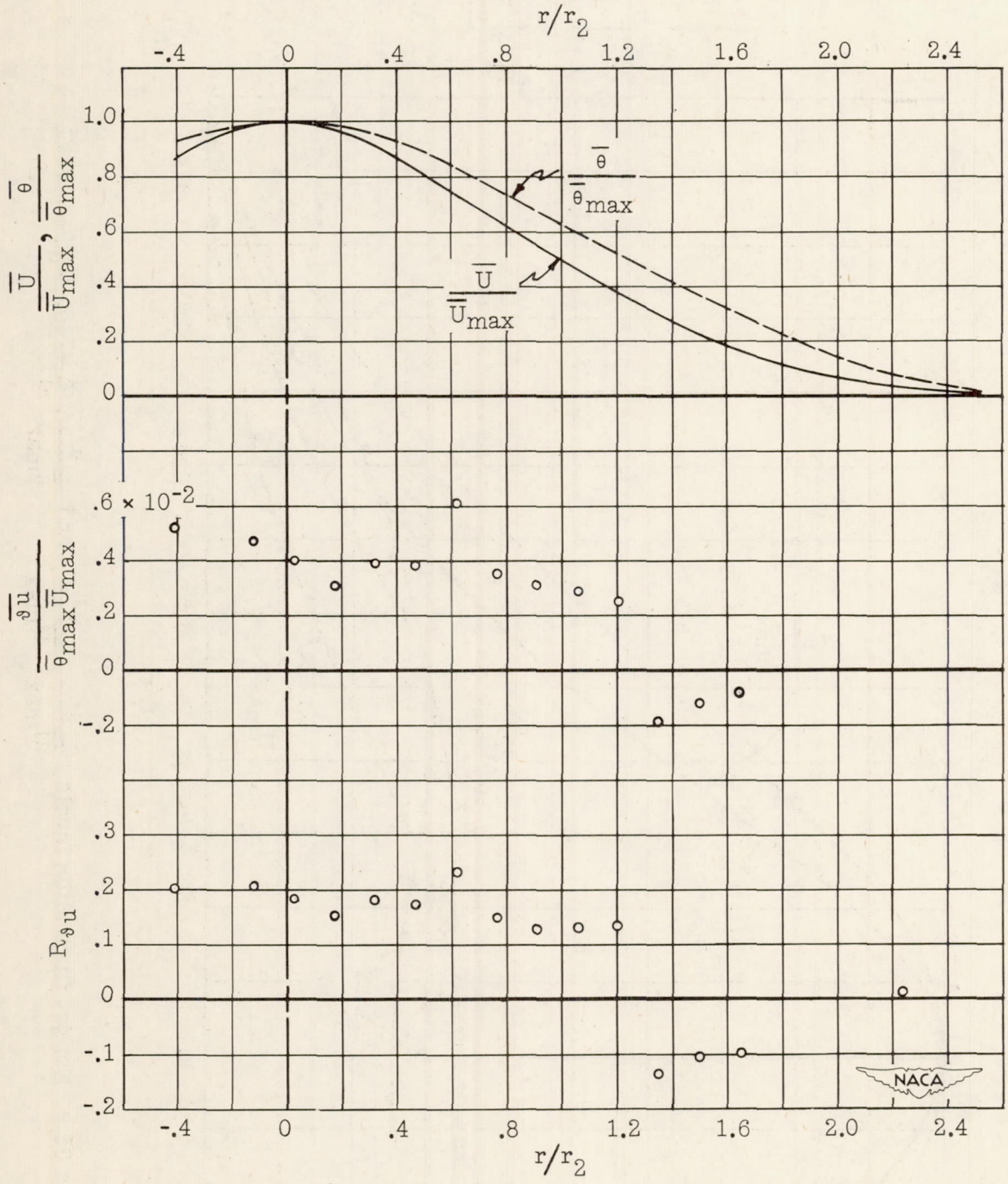

Figure 24.- Hot-jet $\overline{\vartheta u}$ correlations. $\frac{x}{d} = 15$; $\overline{\theta}_o = 170^\circ$ C.

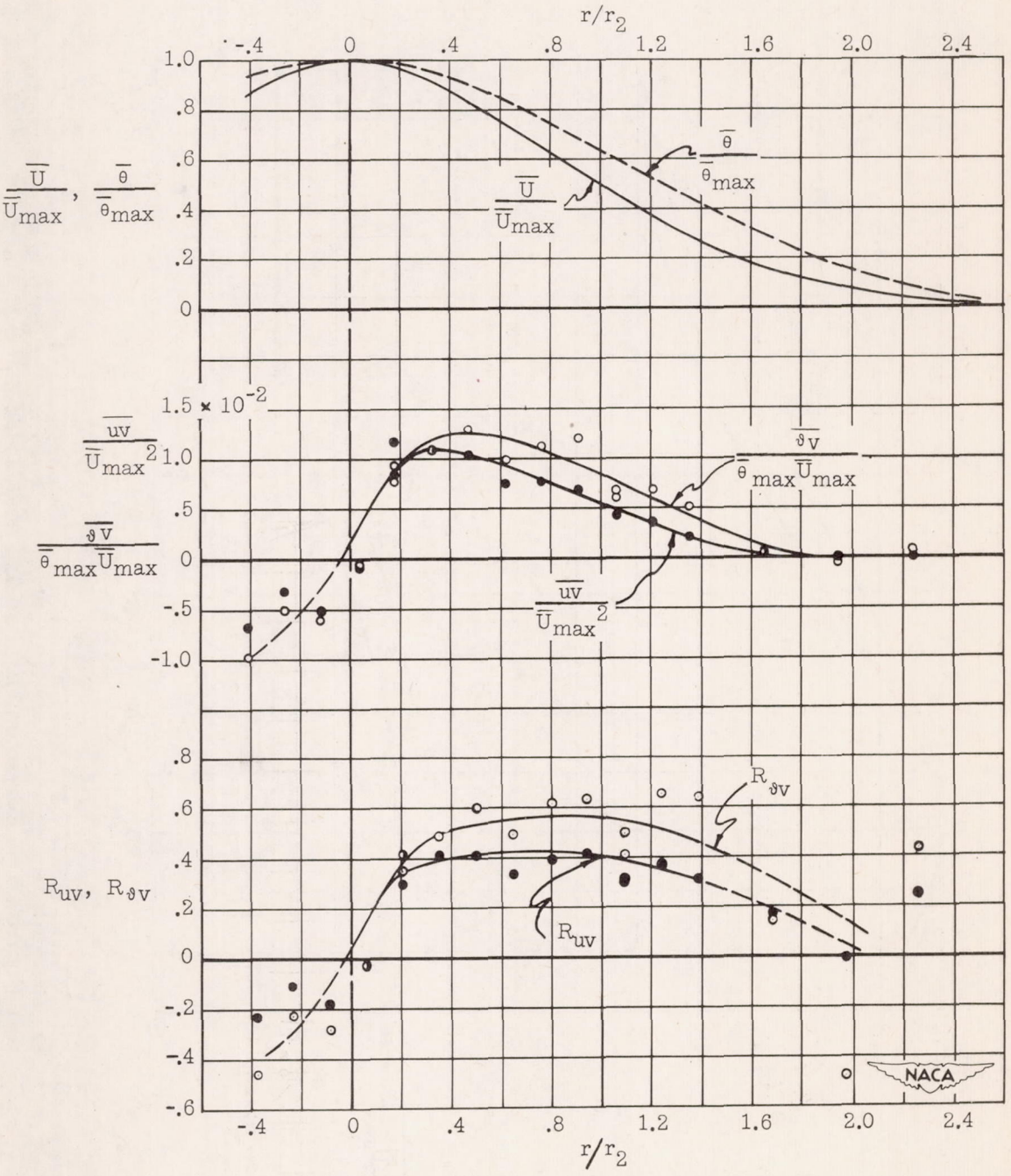

Figure 25.- Hot-jet double correlations. $\frac{x}{d} = 15$; $\overline{\theta}_o = 170^\circ$ C.

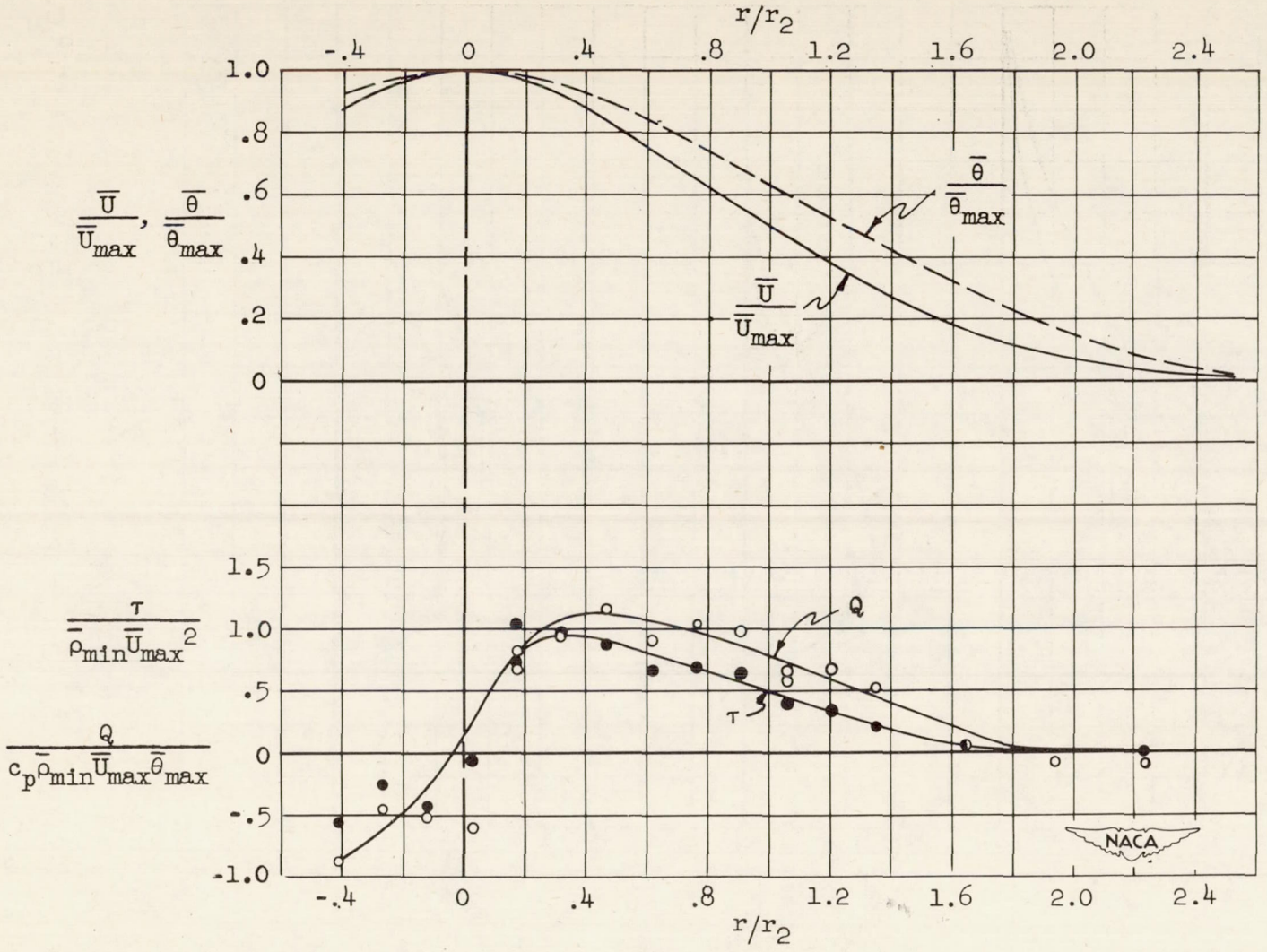

Figure 26.- Hot-jet momentum and heat transfer. $\frac{x}{d} = 15$; $\bar{\theta}_o = 170^\circ$ C.

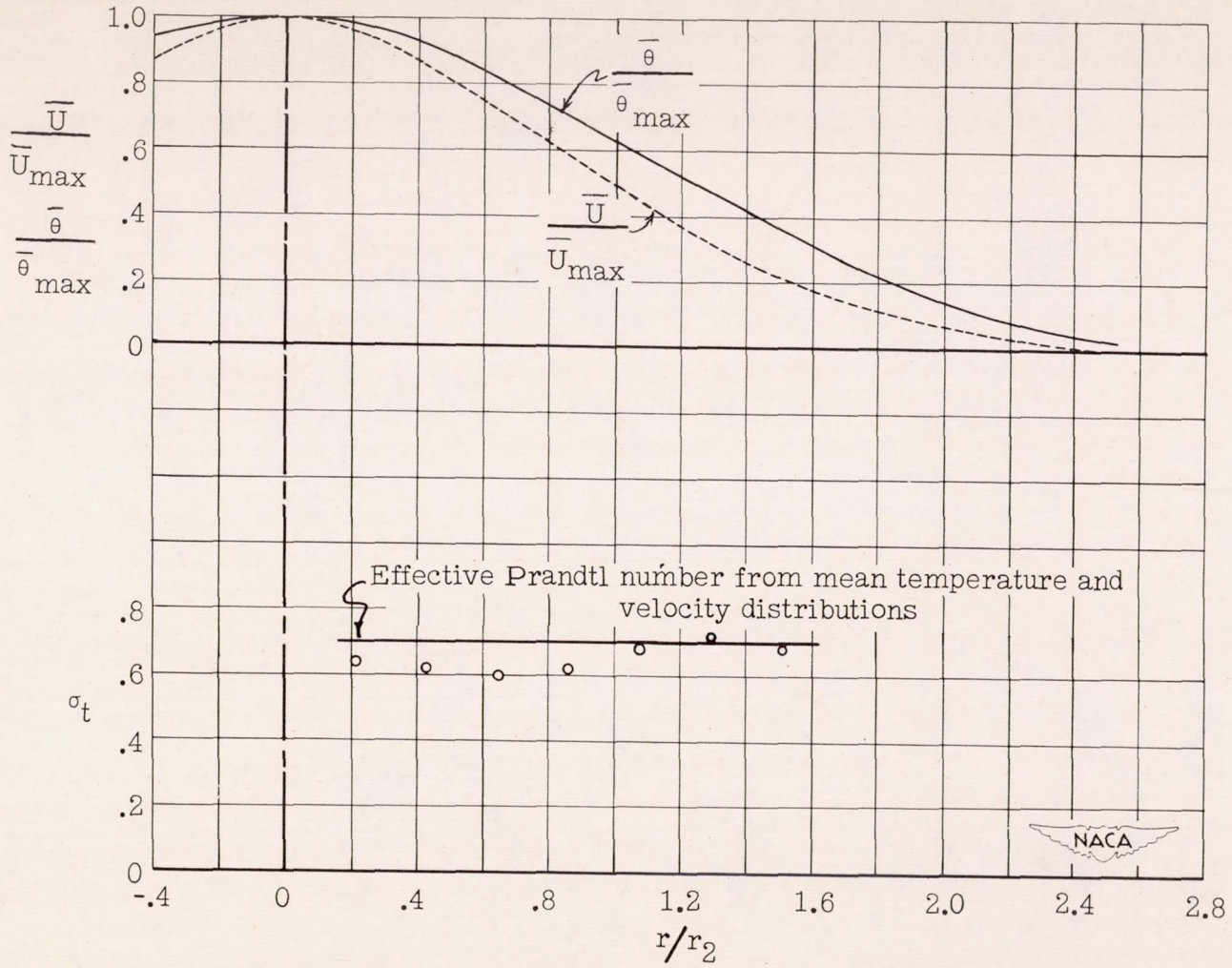

Figure 27.- "Turbulent Prandtl number." 1-inch hot jet. $\frac{x}{d} = 15$; $\bar{\theta}_o = 170^\circ$ C.